Synthesis of a BioMEMS Device for Direct Delivery of Cancer Drugs

Andrew U. Abreu

Materials Science and Engineering, Rensselaer Polytechnic Institute

NNIN REU Site: Howard Nanoscale Science and Engineering Facility, Howard University, Washington, DC
NNIN REU Principal Investigator(s): Dr. Gary Harris, Howard Nanofabrication Facility, Howard University
NNIN REU Mentor(s): Nefertiti Patrick-Boardley, Applied Physics, University of Michigan
Contact: abreua@rpi.edu, gharris@msrce.howard.edu, boardley@umich.edu

Abstract:

This project focused on optimizing the fabrication process of a biological microelectromechanical systems (bioMEMS) device for direct delivery of cancer drugs. A photolithographic process was used to fabricate 50 × 50 μm "step" groove patterns on aluminum substrates, which were then used to make a metal mold for device synthesis with the inclusion of grooves. Heat was incorporated during PDMS curing to drastically reduce production time.

Introduction:

Direct delivery of cancer drugs is a topic of increasing importance, as current methods of cancer treatment are expensive and inefficient. High concentrations and large dosages are required for chemotherapy drugs and other substances to have a significant effect in treating cancer, driving up treatment costs as chemotherapy drugs are expensive to make. Direct delivery of cancer drugs increases the efficiency of treatment, lowers the costs as less drugs and lower concentrations are required, and reduces the severity of side-effects.

One method for implementing direct delivery is to implant a biocompatible device made of polydimethylsiloxane (PDMS) containing cancer drugs into sites of recently removed tumors. The drugs are dispensed from a hydrogel inside the device, using a hyperthermia coil to supply heat for activating the gel's contraction mechanism, with micro-channels acting as delivery pathways for drug flow.

This project focuses on the inclusion of microgrooves onto the device surface for cell attachment, fostering biocompatibility with the human body. The grooves can be tailored to the average size of the specific cancer cell type for optimum cell adhesion.

Procedure:

SU-8 50 microgrooves were made on 0.5 in × 0.5 in aluminum 5052 alloy substrates of thickness 0.3 mm, following the procedures outlined by MicroChem for 50 μm films [1]. It should be noted that: the final ramp-up spin speed was ~ 2180 RPM; all bakes were done in convection ovens, so heating times were 50% longer than outlined in procedures; and a hard-bake of 2 hrs minimum was carried out on the aluminum substrates. After making four substrates, a mold was assembled so that the bottom had a cylindrical piece of metal with diameter of 0.6-0.7 cm and height of 0.9 cm, and the interior length and width (on the inside of the mold) was 1 cm each, with the height at 1.1 cm. Under a fume hood, the mold was placed on a Petri dish with a few drops of silanizing agent. The dish was placed into a vacuum desiccator and was left in chamber for 1 hr under a pressure of 12.5 psi.

Two pieces of aluminum foil were molded onto the bottoms of 250 ml and 150 ml beakers. Using materials from a 184 Sylgard kit, PDMS was prepared by mixing at a weight ratio of 10:1 monomer to curing agent on a chemistry boat. Once the mixture became cloudy due to bubbles, the boat was degassed in vacuum at 12.5 psi for 45 min. Afterwards, any remaining bubbles were removed and the mold was placed on large foil boat. Next, the mixture was poured into a mold and small foil boat and re-degassed at 12.5 psi for a minimum of 1 hr, with pressure throttled every 20 min to assist with bubble removal. The boat was then placed on a hot plate, set to 125°C, for 20 min until the PDMS cured. After air cooling,

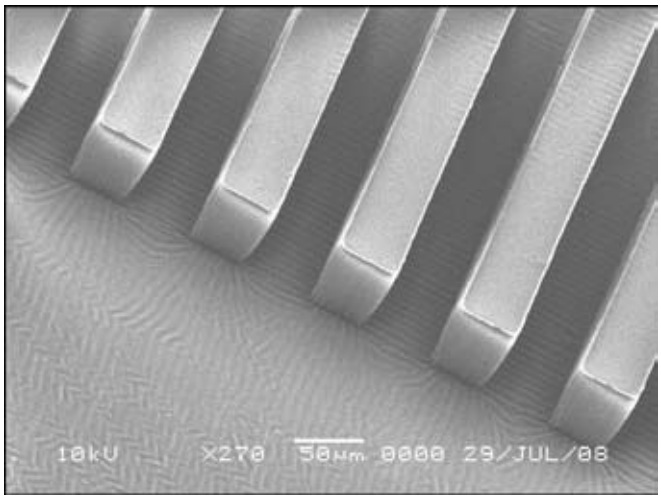

Figure 1: SEM of PDMS replica of microgroove pattern.

the mold was disassembled, using a razor to remove excess PDMS and foil from the small boat while carefully removing the substrates from casing. Using a micropipette to drop a small amount of curing agent on the side of the casing with a hole, the thin piece of PDMS from the small foil boat was cured onto a PDMS casing at 125°C for 20 min. After an air cool, the excess PDMS was removed using a razor.

Results and Discussion:

Using scanning electron microscopy (SEM) images of PDMS replicas such as in Figure 1, we confirmed the process conditions for good resolution replica molding of SU-8 microgrooves, and then fabricated the casing mold with the substrates. The original processing time, without the addition of heat, was dramatically reduced from 48 hours to 45 minutes with the inclusion of heat during PDMS curing. Figure 2 shows the completed device casing, and Figure 3 demonstrates the successful microgroove pattern replication onto the device surface. A preliminary experiment monitoring the cell attachment to microgrooves was conducted, and initial results showed that cells were in fact attached to the microgroove walls, as shown in Figure 4.

Conclusion:

In conclusion, the process and conditions used were successful in the fabrication of microgrooves on the bioMEMS device surface, potentially allowing the device to integrate with the human body without rejection. Along with the reduction in production time, our findings increase the viability of the device as an alternative to current cancer therapy methods.

Future Work:

For future work, long term studies of cell adhesion to device microgrooves will be conducted, flow-rate measurements of drug delivery via the hydrogel will be obtained, and efficacy of iron-oxide nanoparticles as a potential therapy in conjunction with the device will be determined.

Acknowledgments:

Thanks in part to: Prof. Wole Soboyejo and research group, Princeton University; James Griffin, HNF site coordinator; Nefertiti Patrick, Mentor; Dr. Gary Harris, HNF PI; All HNF staff and faculty; National Nanotechnology Infrastructure Network Research Experience for Undergraduates Program; National Science Foundation.

References:

[1] MicroChem, NANO™ SU-8 Negative Tone Photoresist Formulations 50-100.

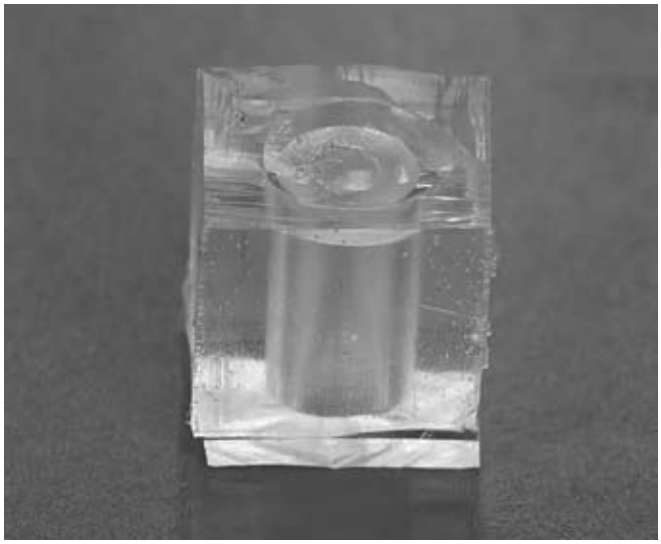

Figure 2: Photo of finished device casing.

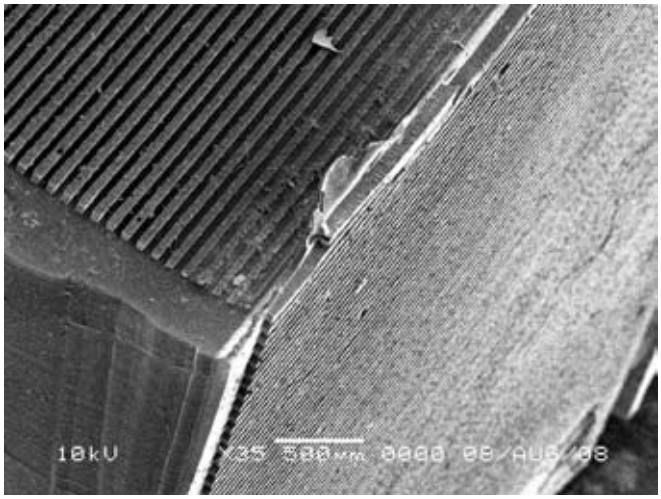

Figure 3: SEM micrograph of a corner of PDMS casing.

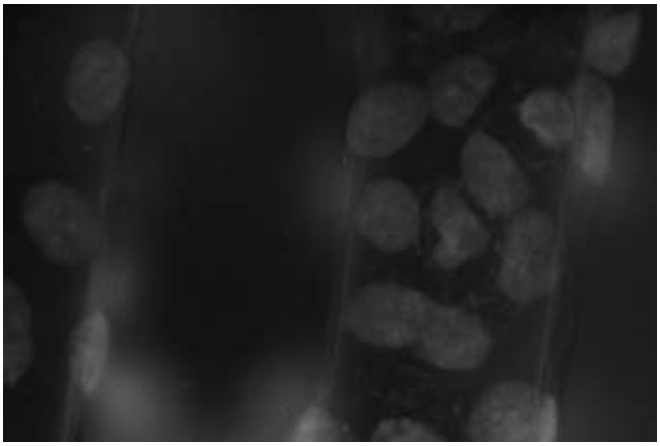

Figure 4: Photo of nuclear-stained cancer cells attached to microgrooves.

Optimizing the Direct Fabrication of Nanoparticles for Cancer Diagnostics

Sophia M. Allaf

Applied Health, Azusa Pacific University

NNIN REU Site: Stanford Nanofabrication Facility, Stanford University, Stanford, CA

NNIN REU Principal Investigator(s): Dr. Mary Tang, Professor Yi Cui, Material Science and Engr, Stanford University

NNIN REU Mentor(s): Ching-Mei Hsu, Stephen Connor, Material Science and Engr, and Chemistry, Stanford University

Contact: sophiaallaf2@apu.edu, mtang@stanford.edu; chingmei@stanford.edu

Abstract:

Nanoparticles with specific ordered structure and composition can produce unique optical or electromagnetic signatures. These nanoparticles are finding new uses such as biomarker scaffolds in cancer diagnostics. This work involved optimizing the process of direct fabrication using nanoimprint and other techniques common to device manufacturing in order to produce these nanoparticles. In particular, our work focused on creating nanoimprint templates and optimizing their use in thermal nanoimprinting. In order to optimize the direct fabrication process, solution phase synthesis and various characterizations, such as scanning electron microscopy (SEM) of metal nano-structures were used [1]. Nanosphere lithography (NSL) of wafer-scale arrays was achieved through Langmuir-Blodgettry (LB) and careful reactive ion etching as shown in Figure 1. We utilized LB in order to bypass many of the limitations of the current fabrication methods and still be able to create close-packed nanoparticle arrays over large scales.

This is unique in the field of NSL and originates primarily in the use of nanoparticles of silica as a direct mask for etching. The motivation behind this research was to develop an optimized method of fabricating magnetic nanoparticles for highly selective and sensitive cancer bioassays.

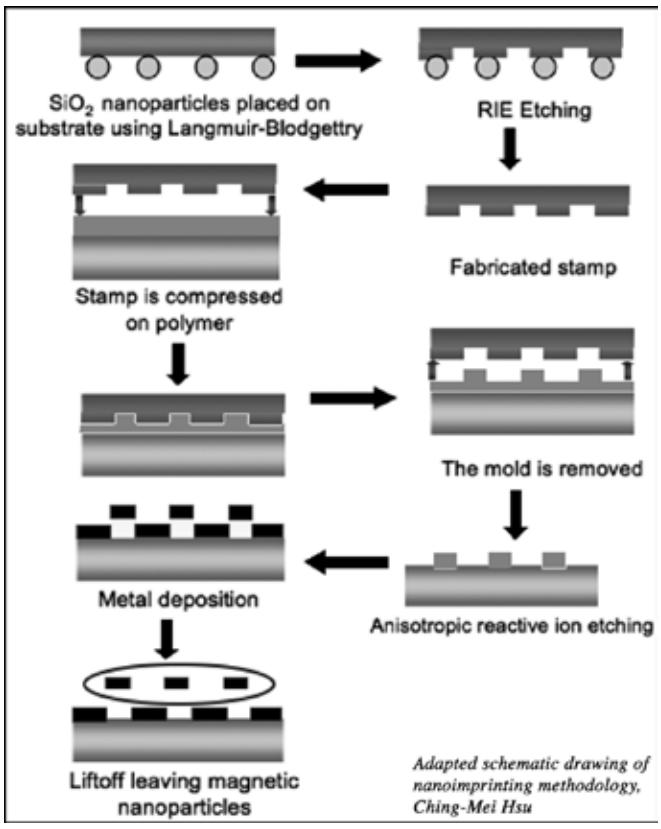

Figure 1: Fabrication of the magnetic nanoparticles.

Introduction:

Magnetic nanoparticles were first developed approximately 35 years ago [1]. These nanoparticles have shown remarkable potential for curing the cancer disease and have brought new dimensions to cancer research. Our group has previously demonstrated the use of the Langmuir-Blodgett (LB) method to produce stamps, and used those stamps for to produce templates for synthetic antiferromagnetic (SAF) nanoparticle fabrication. However, the complete process to use these stamps and templates to produce the SAF nanoparticles has not yet been done. We fabricated stamps which will be utilized in this process so that the SAF nanoparticles can be fabricated and investigated as bioassays for cancer.

In order to enhance the process of direct fabrication, we needed to make high-density arrays of the SAF nanoparticles, which are typically made using either electron beam lithography or photolithography methods. However we utilized the LB method, which is relatively fast, inexpensive and uses only small amounts of raw material, whereas lithography is expensive, time consuming and uses large amounts of raw material. The LB method utilizes the LB trough.

In brief the LB trough, as shown in Figure 2, is an instrument that is used to study the properties of a monolayer of amphiphilic molecules. Among other applications, the instrument can compress the monolayer to deposit LB films on a solid substrate, such as silicon.

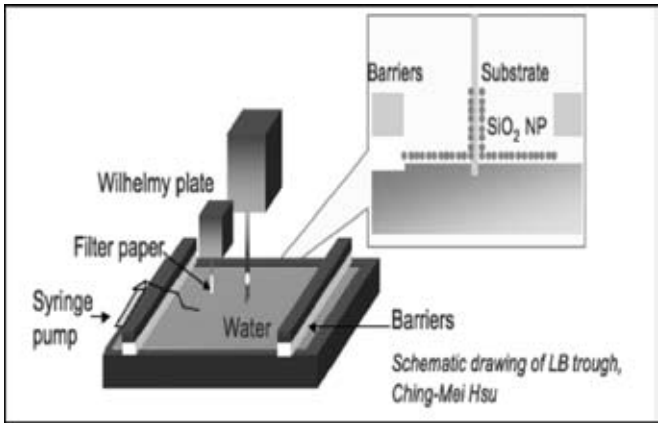

Figure 2: Langmuir-Blodgett trough and deposition.

Utilizing this method we hoped to accomplish our objectives of enhancing the process of direct fabrication using nanoimprint and other techniques, such as the LB trough for deposition, in order to produce uniform arrays of silicon nanopillars across the substrates surface, create many nanoimprint templates in a short amount of time and improve their use in thermal nanoimprinting. Finally we hoped to employ an optimized method of fabricating magnetic nanoparticles for use in highly selective and sensitive cancer bioassays. Our particular research area concentrated on placing the SiO_2 nanoparticles on the Si substrate to be used as etch masks to create silicon nanopillars for nanoimprint templates.

Experimental Procedure:

Functionalization of SiO_2. Two mL of the cleaned silica nanoparticles solution was diluted into 14 mL absolute ethanol 1 mL water, and 100 µL 3-aminopropyl (diethoxymethyl-silane). 97% (APDES) is added with vigorous stirring. The sample was stirred overnight and then heated at 100°C for one hour while being covered in aluminum foil. Cleaning was then performed on the functionalized sample by centrifugation into ethanol and methanol, in 15-minute intervals for a total of five intervals. The solution-based sample was then taken for deposition, with final dispersion into the spreading solvent desired for LB.

Langmuir-Blodgett Deposition. The functionalized samples of silica nanoparticles were injected onto the water subphase by means of a syringe pump. The film was then compressed until a sharp rise was observed in the surface pressure, indicating the formation of a monolayer. Dip-coating depositions were usually performed on oxygen plasma cleaned silicon substrates with the substrate perpendicular to the water surface. The substrate was dipped through the monolayer at 40 mm/min, followed by raising the substrate at 5 mm/min to collect an even film. The surface pressure for optimal deposition was strongly dependent on the size of the nanoparticles, with larger silica samples commonly reaching pressures of 5 mN/m^2.

Results and Conclusions:

It is clearly seen in the SEM image shown in Figure 3 that uniform arrays of masked nanoparticles are evenly formed across the silicon wafer. (See T. Sengupta's report, page 28, for etching the Si using this mask, and producing the stamp.) Thus, the Langmuir-Blodgett method bypassed many of the limitations of the current fabrication methods on the nanoscale. Additionally, we produced close packed arrays of SiO2 nanoparticles by LB deposition. Using this process and subsequent etching, a stamp for the fabrication of magnetic nanoparticles was produced.

Future Work:

In the further experimentation of the LB process, we hope to investigate the limitations of the current functionalization method, such as defects, incomplete coverage and imperfect hydrophilicity that occurs in certain regions of the substrate after deposition. Also, we hope to utilize these stamps to produce magnetic nanoparticles for cancer bioassays.

Acknowledgments:

I would like to thank my mentors Ching-Mei Hsu and Stephen Connor, my PI's Professor Yi Cui and Dr. Mary Tang, our site coordinator Dr. Michael Deal, James Conway, Ben Weil, Maureen Baran and all the SNF processing staff. I would especially like to thank the National Nanotechnology Infrastructure Network Research Experience for Undergraduates Program, Stanford Nanofabrication Facility, National Science Foundation and the Center of Cancer Nanotechnology Excellence for their financial support.

References:

[1] Hsu, C. and S. Connor, Nanosphere Lithography. 2-8 (2007).

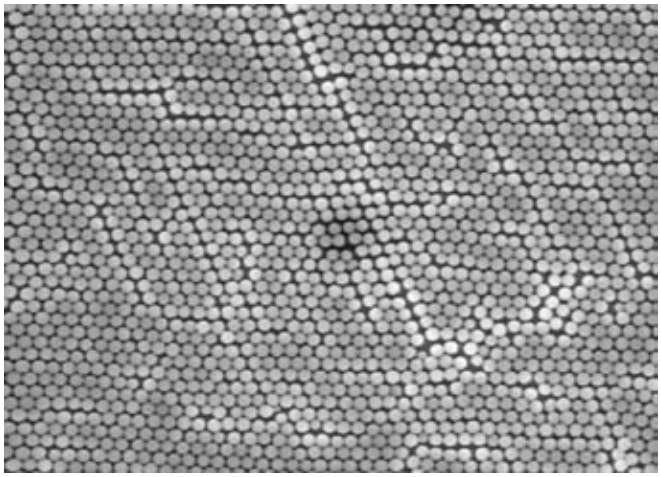

Figure 3: Uniform nanoparticles are formed across the silicon wafer. SEM taken at 25000x.

Optimization of Step and Flash Imprint Lithography: Imprinting a Substrate for One Step Release of Drug Delivery Nanocarriers

Elizabeth Cha

Biomedical Engineering, Johns Hopkins University

NNIN REU Site: Microelectronics Research Center, University of Texas, Austin, TX

NNIN REU Principal Investigator(s): Dr. Krishnendu Roy, Biomedical Engineering, University of Texas at Austin

NNIN REU Mentor(s): Mary Caldorera-Moore, Biomedical Engineering, University of Texas at Austin

Contact: echa4@jhu.edu, kroy@mail.utexas.edu, mcmoore@mail.utexas.edu

Abstract:

Step and flash imprint lithography (S-FIL) is a nanoimprint lithography technique that can be used to fabricate nanoparticles of specific shape, size, and aspect ratio. The Imprio 100 (Molecular Imprints, Austin, TX) is a commercially available S-FIL tool that uses silicon (Si) wafers as the imprinting substrate. To create a suitable imprinting surface that will initially act as an adhesion layer during the imprinting process and then as a release layer to mildly remove the nanoparticles from the surface; the Si wafer is pre-treated with a bottom anti-reflective coating (BARC) and then a water soluble polymer layer: polyvinyl alcohol (PVA). Defects on the imprinting substrate will result in imperfections in the imprints as shown in Figure 3. The objective of this project was to determine the optimal spin coating speed and percent polymer solution of the PVA that yielded a uniform, reproducible pre-coated substrate. Success in the spin coating process allows for a greater area to be imprinted upon and therefore, contributes to the success of the S-FIL process in creating a maximum number of nanoparticles per wafer. Optimization of the imprinting substrate coating process is required to fabricate uniform imprints and therefore more uniform, reproducible nanoparticles.

Introduction:

Nanoscale drug delivery carriers have become more applicable due to their improvements over current small molecule drugs. Nanoscale drug delivery carriers allow for interaction on the cellular level and real time response and release. With precise control of size and shape, nanoscale drug carriers also can allow for better targeting and response meaning smaller doses of dangerous drugs administered to healthy cells. Limitations in current nanocarrier methodology include bottom up synthesis producing poly-disperse particle size, difficulty of *in vitro* / *in vivo* correlation of kinetics and the use of passive targeting through the enhanced permeability and retention (EPR) effect.

Top down manufacturing, using the S-FIL method as shown in Figure 1, allows for incorporation of multiple properties directly into the nanocarriers. Highly mono-disperse nanocarriers of precise sizes and shapes have been developed using this method [1].

Methods/Materials:

The imprinting substrate consisted of two layers: a bottom anti-reflective coating (BARC), which acts as an adhesion layer and prevents backscattering during the imprinting process, and a water-soluble polyvinyl alcohol (PVA) layer that allows for one step release of the particles upon exposure to aqueous solution, as shown in Figure 2. This PVA layer also allows for simple removal of the particles without using mechanical force, therefore preventing damage and loss of the particles. Imperfections in the substrate cause inconsistency in the imprint and difficulty in creating reproducible, uniform imprints (Figure 3).

The objective of this project was to create a more uniform, reproducible pre-coated substrate by determining the optimal spin-coating speed and percent polymer solution of polyvinyl alcohol to create the substrate.

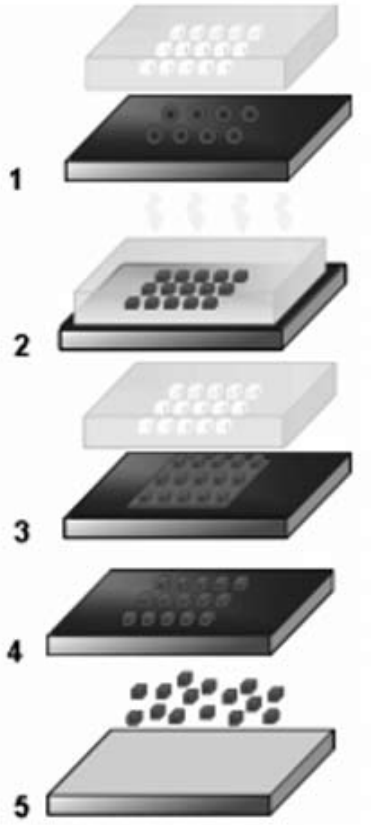

Figure 1: Step and flash imprint lithography method.

1%, 2% and 5% (w/v) polymer solutions of PVA were made by heating distilled (DI) water to 85°C and adding PVA one gram at a time until all was dissolved. The solution was brought up to its correct volume, sealed and left to stir overnight. The next day, the solution was vacuum filtered. To test viscosity, 5 mL of the solution was pipetted into a Canon-Fenske Routine glass viscometer. The solution was timed moving from marks A to B giving the viscosity. Prior to spin-coating, 4 inch silicon wafers were cleaned in a 30 minute piranha solution, a 10 minute buffered oxide etch (BOE) and spun dry for 3.5 minutes. Approximately 650 μL of BARC was spun on a wafer at 2500 RPM for 25 seconds and post baked at 180°C for 1 minute. The wafer was then allowed to sit for ~ 20-30 minutes to allow the BARC coating to dry and the wafer to cool.

Approximately 5,000 μL polyvinyl alcohol solution (PVA) was dispensed onto the center of the wafer. The wafer was allowed to sit for one minute and was then spun for 60 seconds on variable speeds. 1%, 2% and 5% (w/v) polymer solutions were used at speeds of 1000 RPM, 2000 RPM, 3000 RPM and 4000 RPM. Afterwards, BARC and PVA film thicknesses were measured using a Cauchy model with a J. A. Woollam M-3000 ellipsometer.

Results/Conclusion:

As the weight/volume percent (w/v%) of the polymer, PVA 31,000, in the solution increased, the viscosity and refractive index increased proportionally. Higher percent polymer solutions yielded higher average thicknesses at all speeds. An exponential trend was found when examining increasing spin speeds and thicknesses as shown in Figure 4. The 5% PVA polymer had the thickest layers; however, the high viscosity of the solution caused a large amount of air bubbles to form causing multiple imperfections in the substrate. The 1% polymer had such a low viscosity that its average thickness always ranged from 250 to 300 Å regardless of spin speed. Although the substrate was consistently the most uniform and had the least imperfections, the PVA layer was too thin so that particles, when imprinted on the wafer, may still adhere to the BARC. The 2% solution had more imperfections in the substrate than the 1% solution, but its thickness was high enough at speeds of 1000 to 2000 RPM to create a uniform, reproducible substrate. Thus, the 2% polymer was found to be the most ideal concentration to use, while 2000 RPM was found to be the best spin speed to create the least number of imperfections.

Future Work/ Acknowledgments:

In the future, this imprinting substrate will help produce uniform, reproducible imprints, maximizing the number of particles created. I would like to acknowledge the National Nanotechnology Infrastructure Network Research Experience for Research Program and National Science Foundation for funding, and UT Austin, Microelectronics Center, Mary Caldorera-Moore, and my PI, Dr. Krishnendu Roy, for their assistance in completing this project.

References:

[1] Glangchai, L.C., Caldorera-Moore, M., Shi, L. and Roy, K. Journal of Controlled Release 125, 263-272 (2008).

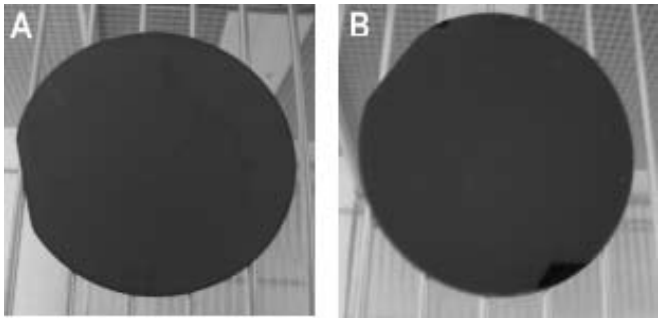

Figure 2: A. BARC coated wafer; B. PVA coated wafer.

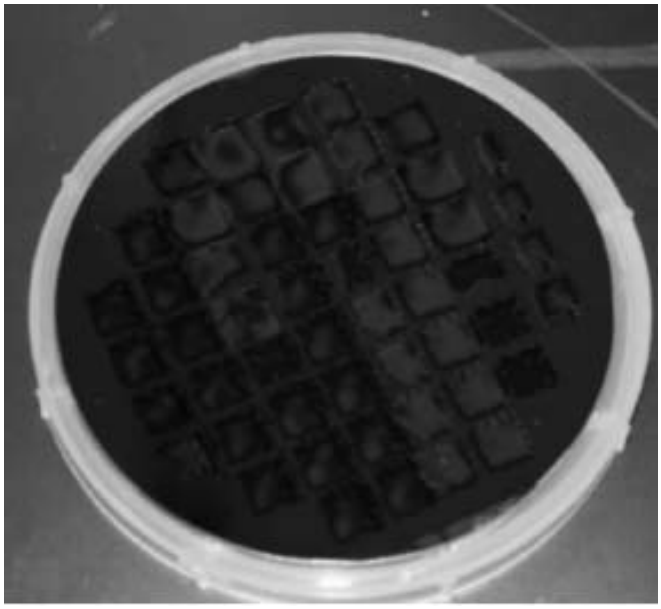

Figure 3: A wafer that has been fully imprinted on. Areas with various coloring show imperfections in the substrate.

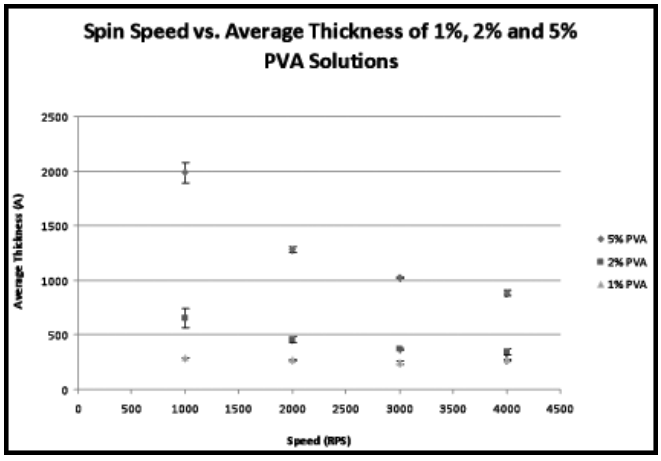

Figure 4: Graph of spin speed vs. average thickness of various percentages of PVA solutions: 5% showed an exponential trend while 2% and 1% polymer solutions had nearly linear trends in thickness.

Optimization and Microfabrication of an Electrosonic Ejector Microarray for Intracellular Nanomaterial Delivery

Allison Connolly

Biomedical Engineering, Johns Hopkins University

NNIN REU Site: Microelectronics Research Center, Georgia Institute of Technology, Atlanta, GA

NNIN REU Principal Investigator(s): Dr. Andrei G. Fedorov, Mechanical Engineering, Georgia Institute of Technology

NNIN REU Mentor(s): Dr. J. Mark Meacham, Mechanical Engineering, Georgia Institute of Technology

Contact: aconnol2@jhu.edu, andrei.fedorov@me.gatech.edu, jmarkmeacham@gmail.com

Abstract:

This REU project focused on optimization of the electrosonic ejector microarray (EEM) to enable efficient intracellular nanomaterial delivery. The EEM ejects biological cells through microscopic nozzles with incorporated electroporation electrodes, thereby opening pores in the cell membrane for uptake of drugs and/or genes/nucleic acids. The device assembly consists of a piezoelectric transducer for ultrasound generation, a polydimethylsiloxane (PDMS) chamber for holding the biomolecule and cell solution, and a 20 × 20 array of pyramidal-shaped nozzles etched in silicon and coated with gold. The piezoelectric transducer drives the sono/mechanoporation of the cells, while the gold-coated nozzles are used to generate an electric field, which allows for electroporation. The PDMS serves as both a fluid reservoir and a microfluidic device. The water in the reservoir transfers the generated acoustic waves from the piezoelectric to the cell mixture, and fluidic channels that are cast into the PDMS allow separate groups of nozzles to be accessed for simultaneous ejection of multiple samples.

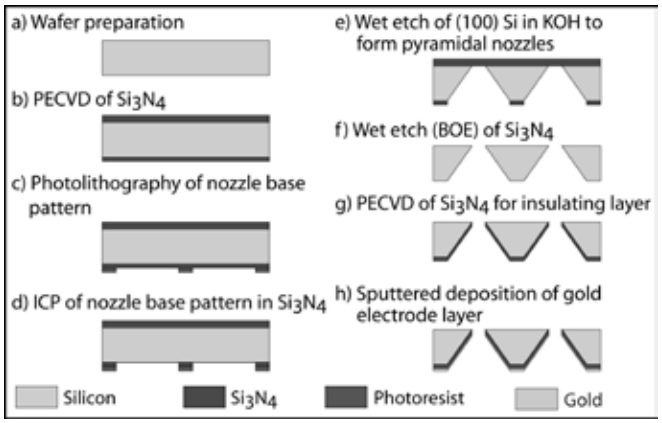

Figure 1: Electrosonic ejector microarray fabrication process.

Device Fabrication:

The fabrication process for the EEM is shown in Figure 1. An array of square openings for the nozzle bases was patterned in Microposit SC 1827 photoresist. This pattern was then transferred into a silicon nitride (Si_3N_4) layer on the backside of a [100]-oriented silicon wafer using inductively coupled plasma (ICP) etching. The pyramidal nozzles were formed by wet etching through the silicon wafer in a potassium hydroxide (KOH) solution (see Figure 1e). The KOH solution etched the [100] orientation (normal to the wafer face) significantly faster than the [111] orientation (54.74° to the wafer face). The size of the nozzle apertures was controlled by varying the etch time. Following the KOH etch, a 500 nm silicon nitride layer was deposited to insulate the silicon nozzles from the gold electrode layer. For better adhesion, a titanium seed layer was sputtered onto the nitride before depositing the gold.

PDMS was selected for its mechanical properties (e.g., high flexibility and compressibility), biocompatibility, and low cost. The PDMS spacer separates the disposable EEM from the remainder of the assembly, maintaining a sterile environment for the cell mixture. The fluidic channels are designed to isolate small groups of nozzles, minimizing sample volumes while maximizing throughput. A mold for the channels is patterned in SU-8 10 on a silicon wafer [1].

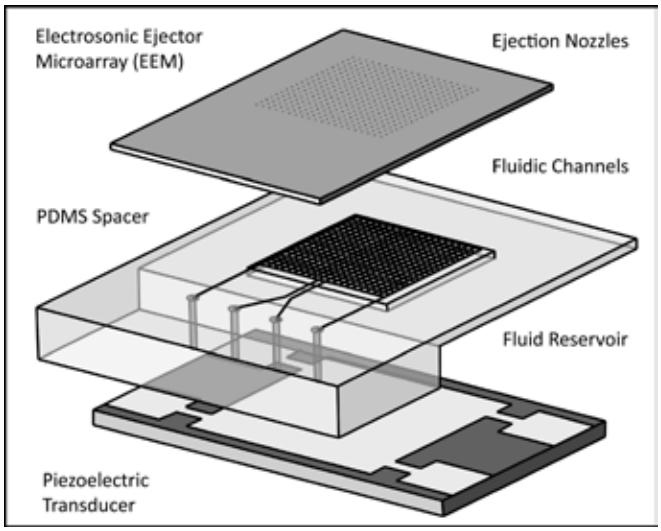

Figure 2: Expanded device assembly.

Trimethylchlorosilane (TMCS) is vacuum desiccated onto the mold to ease removal of the PDMS and allow the mold to be reusable. The fluid reservoir lays flush with the piezoelectric (see Figure 2) and transfers the acoustic waves into the cell medium in each of the nozzles. Although the acoustic properties of PDMS are similar to those of water and the cell medium, the PDMS layers dissipate acoustic energy. Thus, a higher amplitude signal is required to achieve ejection.

Cell Treatment:

The three-layer device assembly can be seen in Figure 2. The cell mixture is fed into the nozzles through the inlet holes in the spacer. We first apply a direct current (DC) to the gold layer generating an electric field in the sample within the nozzles. The electric field causes the polarized cell membrane to break down and separate leading to pore formation and growth [2]. We apply an alternating current (AC) signal to the piezoelectric transducer, which converts electrical oscillations to mechanical motion. The pyramidal shape of the nozzles focuses the generated acoustic field at the aperture. Significant velocity gradients occur only within the aperture and not within the remaining cell mixture. Here, pressure and shear act to both increase the size of the membrane pores and to eject the sample from the device [3]. While the pores are open, nanomaterials enter the cell via diffusion. The solution is ejected into a Petri dish where the membranes refuse, capturing the nanomaterials inside the cell.

Conclusions:

We have shown that a multifunctional device can be fabricated. The modified EEM can combine electroporation with sono/mechanoporation for dual treatment of the cell sample (see Figure 3). Cell ejection was performed using the original EEM to prove that mechanoporation occurs. Figure 4 shows cell uptake of calcein (bottom left) and cell death (bottom right). With the multifunctional device, these factors should be optimized. Due to its acoustic properties and biocompatibility, PDMS was an ideal material for the microfluidic spacer.

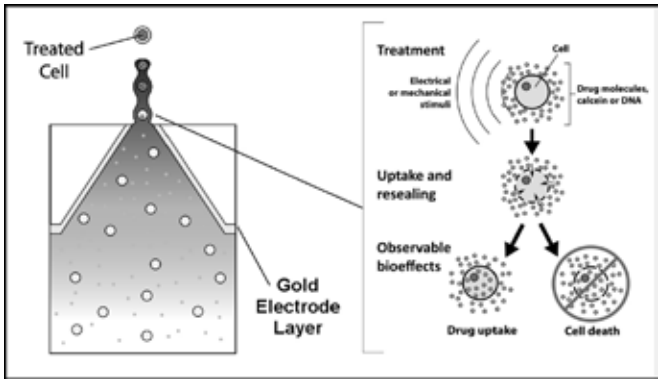

Figure 3: Cell treatment—combining electroporation and mechanoporation.

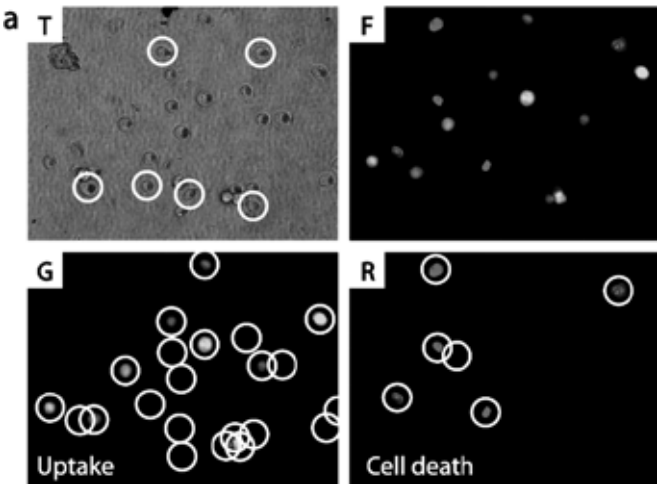

Figure 4: Uptake and viability experiments with calcein (G) and propidium iodide (R) stains.

The spacer reduces cost by minimizing sample sizes and separating disposable parts from reusable ones. Overall, the fabrication of the EEM and spacer is flexible, which allows for parametric optimization for each specific cell line.

Future Work:

In order to characterize the EEM for drug delivery, cell uptake and viability experiments will be conducted with the optimized device. The small fluorescent molecule calcein will be used to evaluate delivery efficiency. Post-ejection staining with propidium iodide will test for cell viability, marking cells whose membranes have not refused. After optimization of ejection parameters (e.g., applied voltage and aperture size), the device will be used for gene transfection with difficult cell lines. We hope to treat glioblastoma cells that are resistant to gene therapy using traditional methods by exploiting the multifuncitonality of the EEM.

Acknowledgements:

The author would like to acknowledge all of those involved in the National Nanotechnology Infrastructure Network Research Experience for Research Program for their help and support, including, but not limited to; James Meindl, Andrei Fedorov, and Mark Meacham.

References:

[1] MicroChem; "Nano™ SU-8: Negative Tone Photoresist Formulations 2-25" (2002).

[2] Gehl, J; "Electroporation: theory and methods, perspectives for drug delivery, gene therapy and research"; Acta Physiologica Scandinavica, 177, 437-447 (2003).

[3] V.Zarnitsyn, J.Meacham, M.Varady, C.Hao, F.Degertekin and A.Fedorov, "Electrosonic ejector microarray for drug and gene delivery," Biomedical Microdevices 10, 299-308 (2008).

Nano-Scale Fluidics for Ultra-Compact Lab-On-A-Chip Device Applications

Ryan Edwards

Biomedical Engineering, University of Oklahoma

NNIN REU Site: Microelectronics Research Center, Georgia Institute of Technology, Atlanta, GA

NNIN REU Principal Investigator(s): Dr. Ali Adibi, Electrical and Computer Engineering, Georgia Institute of Technology

NNIN REU Mentor(s): Dr. Siva Yegnanarayanan, Electrical and Computer Engineering, Georgia Institute of Technology

Contact: ryan.h.edwards-1@ou.edu, ali.adibi@ece.gatech.edu, sivay@ece.gatech.edu

Abstract:

Ultra-high quality factor (*Q*) chip-scale silicon nitride (SiN) optical microresonators are very attractive for lab-on-a-chip biological sensing. Two key challenges in developing multiplexed sensor arrays are fluidic sample delivery and surface coating of the sensor surface. This project focused on designing, fabricating, and testing various SU8 microfluidic channels tightly integrated on the top of an array of SiN microresonators. Each resonator was functionalized with a specific surface coating for a particular analyte, using a large-angle surface patterning tool and the Nano eNabler™ System from BioForce Nanosciences, Inc. Fluidic channels were sealed by a polydimethyl-siloxane (PDMS) or glass cover slip and inlet/outlet ports were provided for the sample injection through external syringe. Preliminary experimental results, obtained by flowing a set of Brix fluids in the microfluidic channel with different refractive index units (RIU), showed that the sensor bulk refractive index sensitivity was ~ 1 nm/RIU.

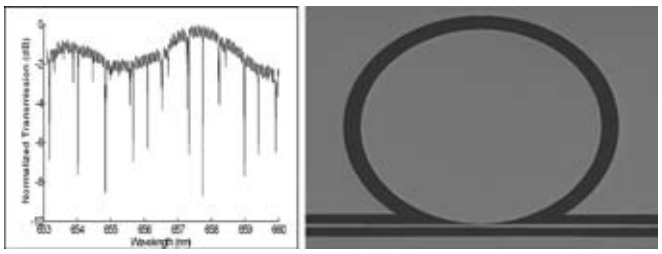

Figure 1: (a) Measured spectral response for an SiN resonator. (b) SEM picture of resonator. The resonator had a diameter of 40 µm.

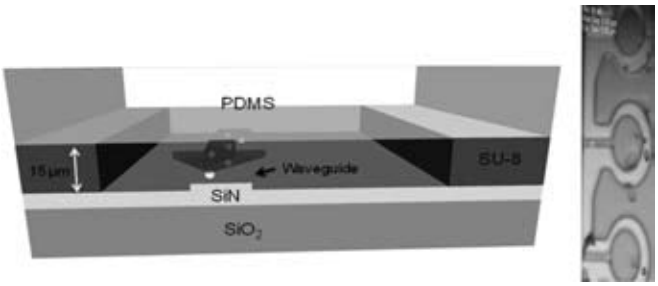

Figure 2: (a) Design of microfluidic channel. The dots on the surface of the SiN waveguide represent surface coatings that will target specific biomolecules that we would like to sense in the fluid. The arrow represents the light that couples to the waveguide. (b) In situ spotting technique was developed using angled 10 mm cantilever tips and a Nano eNabler™. We obtained < 1 µm spots on the active surface of the SiN resonator inside SU-8 microfluidic channels with good spatial overlap to the electromagnetic mode of the resonator.

Introduction:

Our goal is a compact, handheld, lab-on-a-chip device for rapid biomolecular assay. Today, such an assay takes anywhere from a few hours to a week. Using the proposed sensor, we anticipate a biomolecular assay for a multiplexed panel of analytes could be completed within a few minutes from raw serum samples and without cumbersome pre-processing steps such as fluorescent tagging and labeling.

The sensing mechanism relies on the shift in the resonance wavelength of a planar ultra-high *Q* SiN optical resonator induced by changes in the refractive index on the sensor cavity surface (see Figure 1), and is calculated using

$$\lambda_{resonance} = \frac{L}{m} n_{eff}$$

where λ is the resonance wavelength; L, the length of the cavity; m, the mode (1, 2...); and n_{eff} is the effective refractive index of the resonant mode.

In a multiplexed sensor array, each sensor surface has a unique surface coating for sensing a specific biomolecule. In this work, we have developed techniques to solve the two major challenges in developing such a multiplexed sensor. The first involves the development of optimal microfluidic channels fabricated directly on the top of the SiN resonators that enable dramatic reduction in the diffusion time for the biomolecules thereby enabling assay time to be dominated mostly by the binding kinetics on the sensor surface. The second task in this research involves the development of surface patterning techniques that could enable highly-specific surface coatings to be applied to the sensor surface following the fabrication of the fluidic channels.

Experimental Procedure:

SiN resonator chips were fabricated using electron beam lithography. They were operated in the visible wavelength range to overlap with the low optical absorption loss region for water. SU-8 (MicroChem) was spin-coated on the SiN resonators to a thickness of 15 μm and patterned to define microfluidic channels pre-aligned to the resonators (see Figure 2a).

A large-angle surface patterning tool and the Nano eNabler™ System was used to print sub-femtoliter volumes directly on the surface of the resonators within the microfluidic channels. We repeatedly approached < 1 μm protein buffer spots on the top of the SiN resonator, by optimizing the approach velocity and dwell times for the surface patterning tool. We could also achieve a good alignment between the spot and the peak in the electromagnetic mode in the resonator (see Figure 2b).

Finally, we explored several different fluidic channel sealing techniques. One approach was to use a rectangular piece of PDMS (Sylgard 184), treated in oxygen plasma and then attached on the top of the SU-8 microfluidic channel. Another approach that we adopted was direct SU-8 to SU-8 bonding using a SU-8 coated glass cover slip. Prebaking conditions were optimized to enable good bonding. A blanket UV-exposure was used to cure and finally seal the cover slip to the fluidic channel. More optimization of this process is required in order to get a repeatable tight fluidic seal and to avoid fluid leaks.

A prototype sensor consisting of a SiN resonator with a SU-8 microfluidic channel and a PDMS lid was used to evaluate

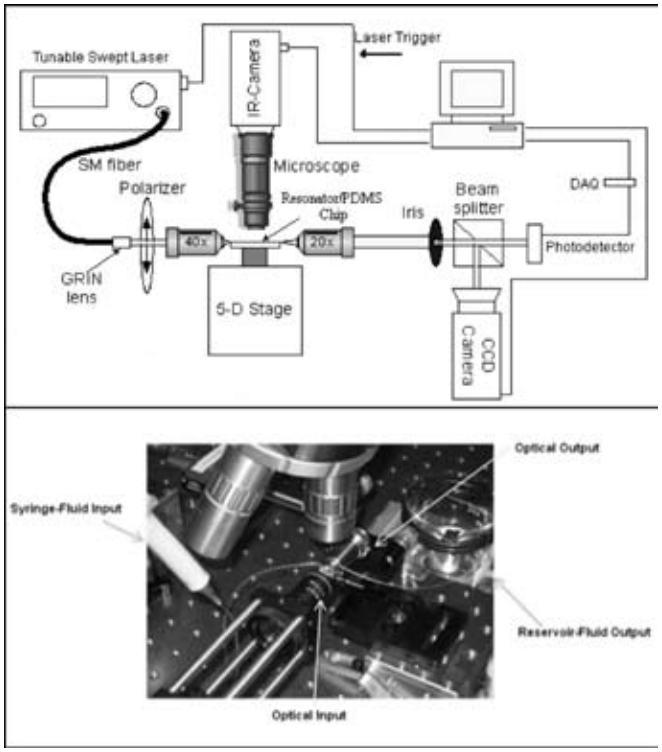

Figure 3: (a) Schematic of optical test setup. (b) Picture showing prototype sensor test using a syringe for fluid injection.

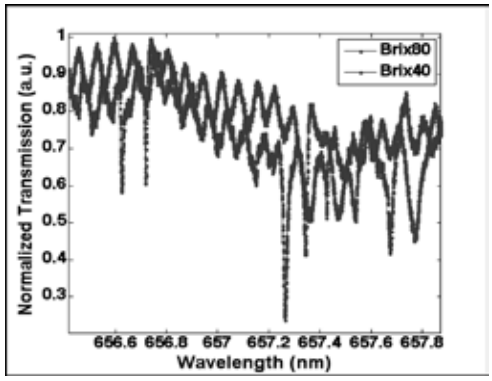

Figure 4: Spectral response of microdisk resonator. Bulk refractive index sensitivity of ~ 1 nm/RIU was experimentally obtained.

initial sensor bulk refractive index sensitivity using Brix fluids injected into the microfluidic channel (Figure 3b). Following fluid injection, the resonance wavelength was obtained by a swept-wavelength test using a tunable laser (New Focus Velocity 650-660 nm) (Figure 3a). We obtained a bulk refractive index sensitivity of ~1 nm/ RIU (Figure 4). Leaking was observed from the PDMS fluidic seal with prolonged fluid flow and resulted in incomplete removal of fluid and even fluid mixing in the sensor. We anticipate that with a more stable fluidic sealing, fluidic mixing could be eliminated and the sensor sensitivity could be improved.

Results and Conclusions:

SU-8 microfluidic channels were fabricated directly overlapping SiN microresonators. A technique suitable for fabricating multiplex-sensor arrays was developed by depositing sub-femtoliter volumes of surface coating ligands directly onto the resonator surface within the microfluidic channel. Due to ease of fabrication, PDMS to SU-8 seal using oxygen plasma was adopted in this project for the first sensor prototypes. Bulk refractive index sensitivity of ~ 1 nm/RIU was experimentally obtained. Better fluid sealing is required in order to prevent leaks and fluid mixing in the sensor.

Future Work:

One way to improve the fluidic seal would be to use a cover slip. An initial process for such a sealing has been developed by using SU-8 coated glass cover slip and exploiting the SU-8 to SU-8 bonding process to directly seal the SU-8 fluidic channel with the glass cover slip.

Acknowledgements:

I would like to express my appreciation to the NSF, NNIN REU Program, and Georgia Tech for their funding and facilities. I would like to express my gratitude towards the site coordinator, Jennifer Tatham Root, for providing the interns with all necessities and a productive research environment. I would like to give a special thanks to Dr. Siva Yegnanarayanan, Dr. Ali Adibi, and the members of the Photonics Research Group for their guidance, time, and supplies.

Flow Cytofluorometry with a Soft Elastomer-on-Silicon Nano Photonic Device for High-Speed Fluorescence Multi-Spectrum Acquisition

Jose Guevarra

Mechanical Engineering, University of California, Santa Barbara

NNIN REU Site: Lurie Nanofabrication Facility, University of Michigan, Ann Arbor, MI

NNIN REU Principal Investigator(s): Dr. Katsuo Kurabayashi, Mechanical Engineering, University of Michigan

NNIN REU Mentor(s): Steven Truxal, Mechanical Engineering, University of Michigan

Contact: joseg@engineering.ucsb.edu, katsuo@umich.edu, trux@umich.edu

Abstract:

Flow cytofluorometry is an invaluable tool in separating and analyzing biological samples. Applications of this technology include medicine, biology, and Homeland Security. This project fabricated a microfluidics flow cell of polydimethylsiloxane (PDMS) to demonstrate on-chip flow cytometry. The fabricated device allowed for detection of fluorescent beads and discrimination of their relative sizes as they passed the interrogation zone. The use of this flow cell in conjunction with a nano photonic microelectromechanical systems (MEMS) device will lead to real-time measurement of fluorescence spectra.

Introduction:

Traditional multispectral flow cytometry measurements use multiple photomultiplier tubes (PMT) to detect photons of varying wavelengths from fluorescent samples. This approach is costly, requiring complex, bulky optics. Steven Truxal, Yi-Chung Tung, and Dr. Katsuo Kurabayashi have developed a novel MEMS device that uses polydimethylsiloxane (PDMS) as a transparent, flexible nano-grating for diffracting multispectrum light and directing it onto a single photomultiplier tube. Coupled with a well-designed microfluidic flow chamber, the device can be used to realize an on-chip multispectral flow cytometry system.

The object of this project was to fabricate a flow cytometer to generate emission light from fluorescent beads passing through flow cell microchannels as part of our aimed system. This will show whether emission intensities are strong enough for fluorescence spectra measurements.

Fabrication:

The flow cell consisted of a PDMS slab with micro patterns that acted as inflow, outflow, and microchannels. To make the flow cell mold a 20 μm photoresist layer of SU-8 10 was spun onto a 4 inch silicon wafer. The wafer was then exposed at 11 mW/cm^2 for 20 seconds with 365 nm light under a pre-existing lithography mask. The wafer was then developed in SU-8 developer until the high aspect ration "hills" were revealed (see step 2 in Figure 1).

Next, PDMS was mixed using the Sylgard 184 silicone elastomer kit (Dow Corning Corporation, 10:1 base-curing agent ratio). The viscous PDMS was placed in a vacuum for 30 minutes to remove any bubbles. The mold was placed in a handmade, aluminum foil cup; PDMS was poured over the mold, and then cured at 150°C for 10 minutes. The solidified PDMS was then peeled from the mold. The PDMS now had 20 μm deep patterns that act as microfluidics channels.

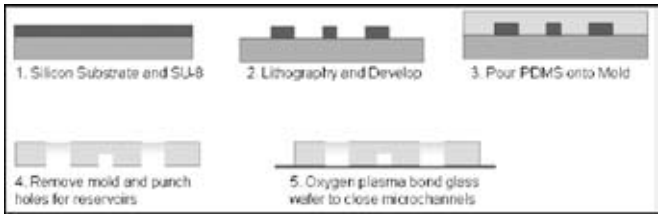

Figure 1: Microfluidics flow cell fabrication.

The mold consisted of several different patterned microfluidic devices. Each was cut from the PDMS to create individual cytometers. Using a 2 mm biopsy punch, holes were punched through the PDMS to create inflow and outflow openings. The PDMS devices were then treated with a O_2 plasma along with a thin glass wafer (250 mT, 80 W, 45 seconds, 17% 2 O, March Asher), then bonded. The flow openings and microchannels were sealed by the glass, leaving openings at the top of the device for inflow and outflow tubing (see Figure 2). Flow cells with channels of 340 μm in width, and 20 μm and 70 μm in depth were fabricated.

Experiment Setup:

The performance of the fabricated microfluidic flow chamber was characterized by observing individual fluorescent beads passing through its microchannel. By measuring the emission light intensity of fluorescent beads, their relative size can be distinguished. Fluorescent beads of diameters 6.5, 31, and

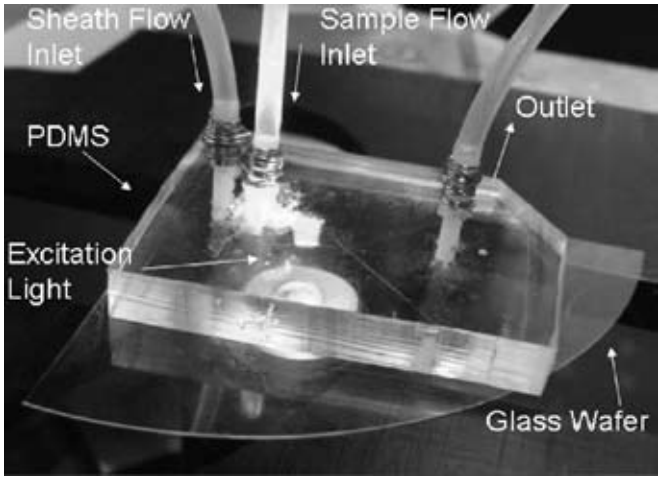

Figure 2: Flow cell excited on microscope stage.

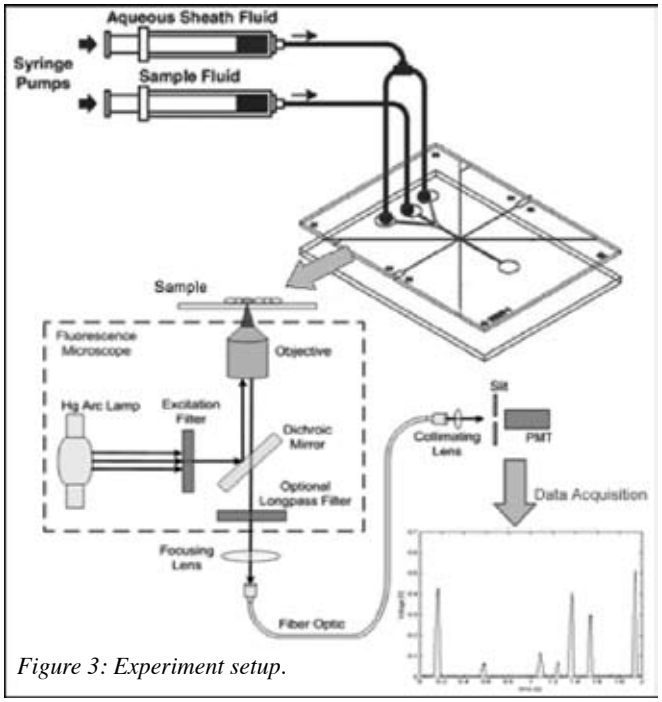

Figure 3: Experiment setup.

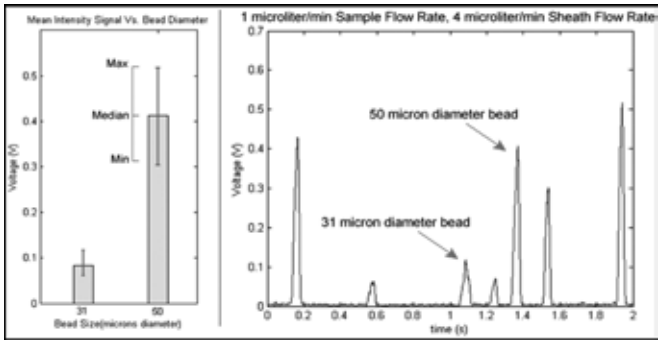

Figure 4: Flow observations.

50 μm were driven through the microchannels. As the beads flowed through the microchannel, they could be observed optically via microscope or the emission light could be directed by fiber optic cable to the PMT for data acquisition (see Figure 3).

Results and Discussion:

The measured intensities provided information on several characteristics of the bead samples and flow cell. The emission intensities could be compared, as in Figure 3, and their relative sizes of the beads could be determined. The mean intensities for 31 μm beads were about 0.9 V and 0.4 V for 50 μm beads. We also determined that 6.5 μm beads require an oil emersion lens to be detected out of the ambient noise in our system.

Conclusion:

We demonstrated simple flow cytometry analysis can be done using MEMS technology. The size of different particles can be determined by their emission light intensity. The measurement error may be reduced by using a two dimensional sheathing flow to direct fluorescent particles closer to the objective lens. Emission light intensity passing through the nano photonic device may be reduced to 10%. Experiments show the emission light intensities are high enough for fluorescence spectroscopy measurements.

Acknowledgements:

National Nanotechnology Infrastructure Network Research Experience for Undergraduates (NNIN REU) Program, the National Science Foundation, and Lurie Nanofabrication Laboratory. I would like to thank Dr. Katsuo Kurabayashi and Steven Truxal for their guidance and help with my project. Thanks to Sandrine Martin and Trasa Burkhardt for their motivation and making the summer a great experience.

References:

[1] Yi-Chung Tung, Katsuo Kurabayashi "PDMS-based opto-fluidic micro flow cytometer with two-color, multi-angle fluorescence detection capability using PIN photodiodes"; Sensors and Actuators B 98 (2004) p 356.

[2] Steven C. Truxal, Yi-Chung Tung, and Katsuo Kurabayashi "High-speed deformation of soft lithographic nanograting patterns for ultrasensitive optical spectroscopy"; Applied Physics Letters; Issue 92, 051116 (2008).

Incorporating Nanocrystals into the Bilayer of Phospholipid Vesicles

Angela L. Holmberg

Chemical Engineering and Chemistry, University of Minnesota-Twin Cities

NNIN REU Site: Microelectronics Research Center, University of Texas, Austin, TX

NNIN REU Principal Investigator(s): Brian A. Korgel, Chemical Engineering, The University of Texas at Austin

NNIN REU Mentor(s): Michael R. Rasch, Chemical Engineering, The University of Texas at Austin

Contact: holmb108@umn.edu, korgel@che.utexas.edu, mr8729@che.utexas.edu

Introduction:

Phospholipid vesicles are useful tools in biotechnology and medicine because of their subcellular size and ability to encapsulate diagnostic and therapeutic molecules. Hydrophobic nanocrystals with useful optical or magnetic properties embedded in the vesicle's lipid membrane could provide a way to control externally the chemical state or the trans-membrane transport rate of molecules trapped inside the vesicle for controlled release of medicine [1], to enhance resolution in magnetic resonance imaging (MRI) [2], or to permit the tracking of vesicles and medicine within the body.

In this project, varying amounts of 1.5-5 nm gold nanocrystals were mixed with lipid and dialyzed to determine the nanocrystals' influence on vesicle formation. Cryo-transmission electron microscopy (cryo-TEM) and TEM images of the vesicle suspensions revealed that gold nanocrystals smaller than the bilayer thickness were primarily embedded within the vesicle membranes, while larger nanoparticles were primarily centered inside lipid micelles. The size-dependence of the incorporation of the nanocrystals into the vesicle lipid bilayer is important to note as vesicle-embedded nanocrystals are investigated further for drug transport, imaging, and controlled release applications.

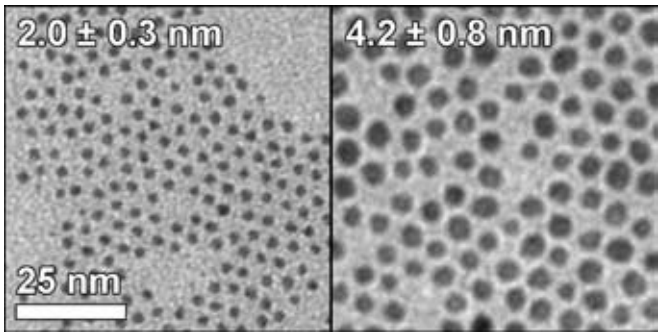

Figure 1: TEM images of separated Au nanocrystals.

Experimental Procedure:

Hydrophobic gold nanocrystals (Figure 1) were prepared as described by Brust [3] by combining a solution of hydrogen tetrachloroaurate in water (0.03 M, 14.4 mL) to a solution of tetraoctylammonium bromide in toluene

(0.2 M, 9.8 mL) and stirring for one hour. Neat 1-dodecanethiol (5 mmols, 1.2 mL) and an ice-cold aqueous sodium borohydride solution (0.4 M, 12 mL) were sequentially added to the organic layer and stirred for an additional hour. Larger Au nanocrystals were synthesized by a similar procedure except the initial solution was reduced by $NaBH_4$ and stirred for four hours before 1-dodecanethiol was added to the organic phase. The resultant Au nanocrystals were centrifuge-washed with methanol at 8000 rpm for five minutes, resuspended in chloroform, and separated by size-selection.

Phospholipid vesicles were synthesized by detergent dialysis for strong membrane integrity and vesicle monodisperity [4]. Egg lecithin (phosphatidylcholine, 0.03 mmols, 0.02 g) and various concentrations and sizes of gold were combined in chloroform and dried under reduced pressure at 40°C. These films were rehydrated with 1 mL of a sodium chloride (0.05 M) and sodium cholate (0.04 M) solution, and equilibrated over two hours with occasional swirling. The lipid solutions were then transferred to wetted dialysis bags and suspended in aqueous NaCl solutions (0.05 M, 0.1 L). The water was changed approximately every four hours over 24 to 28 hours, or whenever possible. Resultant vesicle solutions appeared opalescent or tinted purple or brown depending on the size and concentrations of gold. Carbon-coated copper TEM grids of diluted samples were dried and later stained with uranyl acetate for imaging.

Results and Discussion:

High contrast spots visible in the TEM images (Figure 2) of samples prepared with Au measuring 2.0 ± 0.3 nm in diameter indicate that nanocrystals were incorporated into the vesicles. Unfortunately, due to the dark contrast of the uranyl acetate stain, the small size of the nanocrystals, and the ability of the stain to leak under the edges of the vesicles, it was often difficult to distinguish spots of gold from the stained background. The lipid membrane itself was not stained and therefore not visible either, which made it difficult to determine where exactly the nanocrystals were located relative to the lipid bilayer. As such,

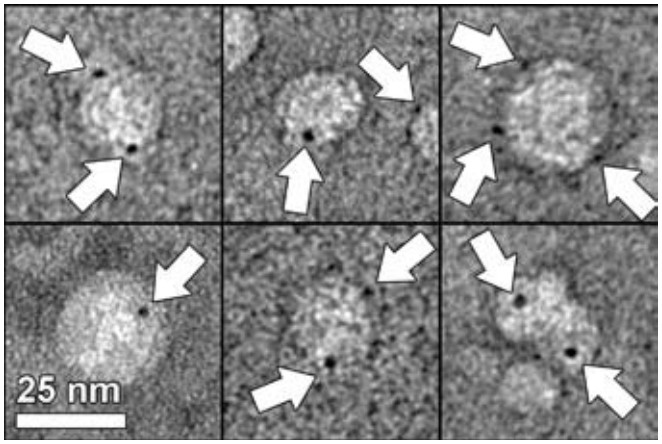

Figure 2: TEM images of stained vesicles with arrows pointing to "small" Au particles.

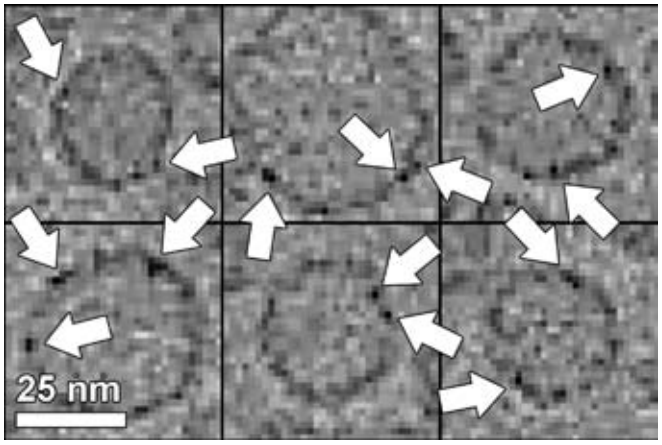

Figure 3: Cryo-TEM images of vesicles with arrows pointing to "small" Au particles.

cryo-TEM (Figure 3) was necessary to better understand how the nanocrystals affected the vesicles. The cryo-TEM images reveal many high contrast spots clearly visible inside the lipid bilayer walls of the vesicles, confirming that the 2.0 ± 0.3 nm Au nanocrystals added at a concentration of 0.3 mg/mL were in fact embedded within the vesicle walls. Nanocrystals were found to aggregate and precipitate out of solution at higher concentrations, and consequently were not analyzed under cryo-TEM. In these cases, there were not enough lipid molecules to completely encapsulate the particles and prevent them from coming in contact with water.

Larger Au nanocrystals measuring 4.2 ± 0.8 nm in diameter behaved somewhat differently. While TEM micrographs (Figure 4) showed that some of the nanocrystals were embedded in the presumed bilayer membrane of vesicles, other nanocrystals appeared trapped in the center of micelle structures. Presumably, nanocrystal-induced bulges in the lipid bilayer equilibrate toward micelles, and crowded lipid molecules in the micelles favor incorporation into the vesicles.

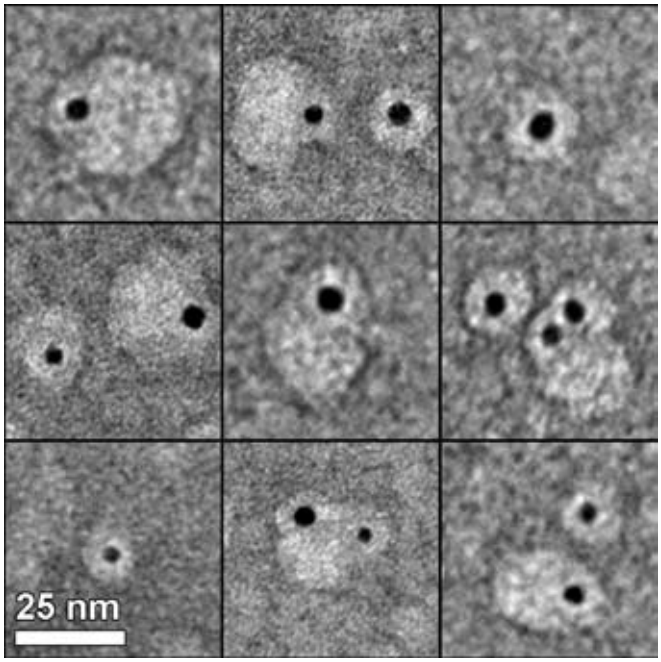

Figure 4: TEM images of a stained vesicle sample with "large" Au nanocrystals.

Future Work:

To further investigate the effect of nanocrystals on vesicle formation, fresh vesicle samples prepared with "large" nanocrystals will need to be synthesized for cryo-TEM analysis. Other future endeavors include incorporating iron oxide nanocrystals into the vesicle walls, and attempting to separate out micelles from vesicles via size-exclusion chromatography.

Acknowledgements:

Much thanks to Dr. Brian Korgel for this opportunity, Michael Rasch for his guidance and support, Jordi Arbiol and his research group at the University of Barcelona for their cryo-TEM images, Jean Toll for her hospitality, and both the National Nanotechnology Infrastructure Network Research Experience for Undergraduates (NNIN REU) Program for funding.

References:

[1] Paasonen, L.; Laaksonen, T.; Johans, C.; Yliperttula, M.; Kontturi, K.; Urtti, A.; "Gold Nanoparticles Enable Selective Light-Induced Contents Release from Liposomes"; J. Cont. Release, 122, 86-98 (2007).

[2] Pankhurst, Q. A.; Connolly, J.; Jones, S. K.; Dobson, J.; "Applications of Magnetic Nanoparticles in Biomedicine"; J. Phys. D: Appl. Phys., 36, R167-R181 (2003).

[3] Brust, M.; Walker, M.; Bethell, D.; Schiffrin, D. J.; Whyman, R.; "Synthesis of Thiol-derivatised Au Nanoparticles in a 2-phase Liquid-Liquid System"; J. Chem. Soc., Chem. Commun., 7, 801-802 (1994).

[4] Korgel, B. A.; Van Zanten, J. H.; Monbouquette, H. G.; "Vesicle Size Distributions Measured by Flow Field-Flow Fractionation Coupled with Multiangle Light Scattering"; Biophys. J., 74, 3264-3272 (1998).

Glass-Frit Bonding for Selective Functionalization and Packaging of Biosensors

Pradeep Hothur

Department of Electrical Engineering, San Jose State University

NNIN REU Site: Microelectronics Research Center, Georgia Institute of Technology, Atlanta, GA

NNIN REU Principal Investigator(s): Dr. Oliver Brand, Electrical and Computer Engineering, Georgia Tech

NNIN REU Mentor(s): Luke A. Beardslee, Electrical and Computer Engineering, Georgia Institute of Technology

Contact: bauerstatus@gmail.com, oliver.brand@ece.gatech.edu, luke.beardslee@gatech.edu

Abstract:

In an effort to enhance diagnostic techniques for diseases, the development of microelectromechanical system (MEMS) biosensors offers a novel approach towards mass producing inexpensive reliable sensors. The objective of this project is to effectively package a biosensor through a glass-frit bonding process using a screen printer. In particular, the process outlined here is meant to work with mass sensitive biosensors; these sensors work by inducing a change in resonant frequency based on the change in mass due to analyte attaching to the sensor, i.e. protein binding. Upon completion of the research, packaging wafers have been successfully micromachined and etch rates and etch rate selectivity for the required silicon etching was established. Furthermore the glass-frit material was successfully screen-printed onto a packaging wafer, which was then bonded to a test wafer. Future work will include bonding a packaging wafer to a wafer with actual sensors.

Introduction:

As a means to test our biosensors, we initially resorted to individually assembling them using die-level packaging; the process involved placing a plastic ring onto the resonator chip to form a sample fluid cavity. This however proved to be ineffective for three reasons. To begin with, it was time consuming to place the plastic rings. Second, the resonators and wire bonds could easily break as a result of inserting the plastic rings by hand. Finally, an exact amount of epoxy had to be placed to glue the rings: too much destroyed the resonators and too little resulted in an insufficient seal. The glass-frit bonding process alleviates these problems utilizing wafer-level packaging. The screen-printing process allows to package many resonators dies at once and greatly diminishes the chances of breaking the resonators. Furthermore, the glass-frit bonding is of interest since it is cost effective process, provides a hermetic seal, and can tolerate the surface roughness on the wafer being bonded.

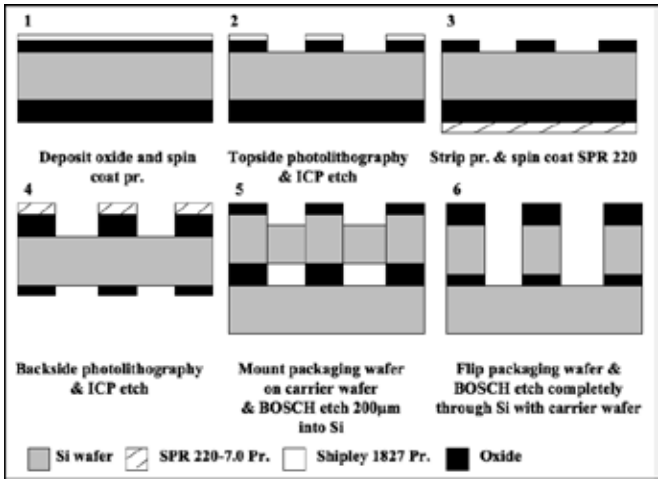

Figure 1: Diagram of fabrication process.

Fabrication:

Fabrication started by depositing 2 μm and 4 μm of oxide on the top and backside of the packaging wafer, respectively. Following standard photolithographic protocols, proximity photolithography and etching in an inductively coupled plasma (ICP) tool were used to pattern the oxide film on the top of the packaging wafer (step 3 in Figure 1). Once we confirmed that the oxide was etched down to the silicon using optical microscopy, we patterned the backside oxide film using a double-side mask aligner (step 4 in Figure 1).

Using the BOSCH process, we then etched 200 μm into the silicon wafer from the topside and then etched completely through the wafer from the backside. This process allowed us to wedge the resonators in the windowed areas on the packaging wafer. Continuing the fabrication, we screen-printed the glass-frit material (DIEMAT, Byfield, MA) onto the packaging wafer (Figure 2). In order to eliminate the organic binder in the glass-frit material, we then went through an organic burnout process. This process step glazed the glass-frit material to the substrate, an initial step towards completing the bonding process. The fabrication was then completed by bonding the packaging wafer to a test wafer.

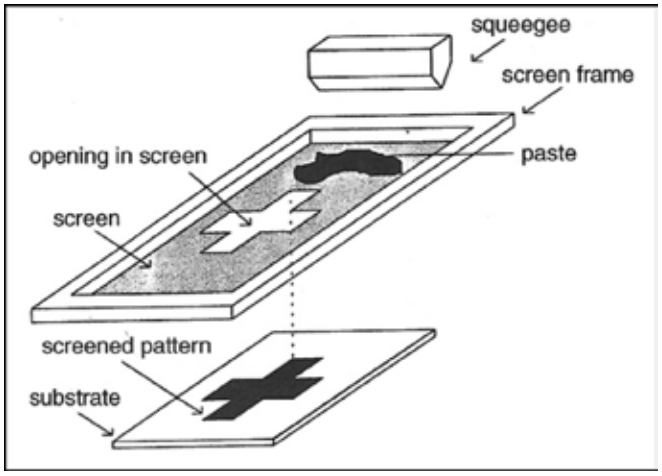

Figure 2: Diagram of screen printer.

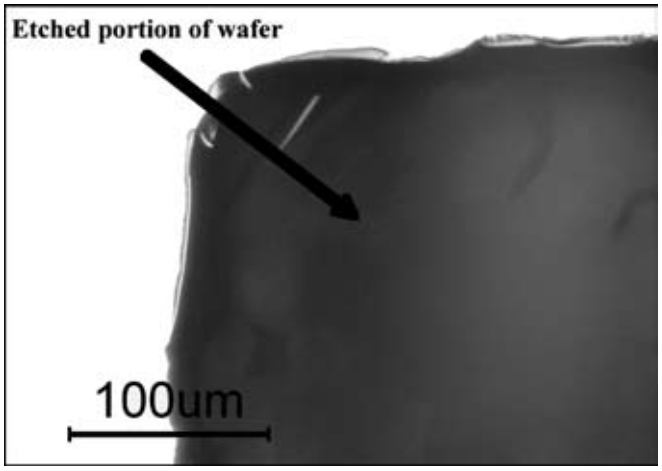

Figure 3: Micrograph of windowed area on packaging wafer after through-wafer etch.

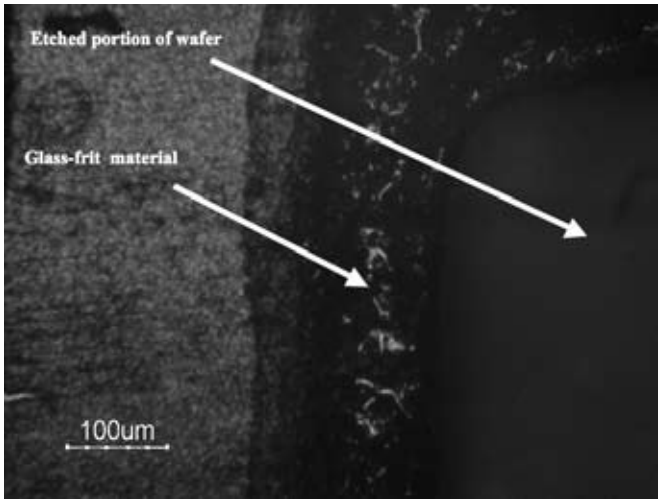

Figure 4: Micrograph of windowed area on packaging wafer after organic burnout and glazing.

Results:

The packaging wafer was successfully fabricated and the fabrication steps were carefully characterized. For the silicon etching with the Bosch process, we acquired an etch rate of 800Å/cycle and an etch rate selectivity to SiO_2 of 178 to 1. Shipley 1827 photoresist was used for the topside photolithography, while Megaposit SPR 220-7.0 photoresist was used for the backside photolithography, due the difference in oxide thickness. The thickness of the screen-printed glass-frit ranged from 30-50 μm. In order to confirm whether this thickness will suffice, the packaging wafer has to be bonded to the device wafer. In the present research, we were able to successfully bond the packing wafer to the rough side of a prime wafer.

Future Work:

We hope to completely characterize the glass-frit bonding process and to bond the packaging wafer to a device wafer with resonant microstructures to acquire fully packaged biosensors.

Acknowledgements:

I would like to sincerely thank my mentor Luke Beardslee, my principal investigator Dr. Oliver Brand, and my site coordinator Jennifer Root. I would also like to thank Dr. James Meindl, the staff of the Microelectronic Research Center, the National Nanotechnology Infrastructure Network Research Experience for Undergraduates (NNIN REU) Program, and the NSF without which this research would not have been possible.

References:

[1] Madou, Marc J. Fundamentals of Microfabrication: The Science of Miniaturization. Boca Raton: CRC Press, 2002.

[2] Hyeong, Jae, and Oliver Brand. "High Q-factor In-Plane-Mode Resonant Microsensor Platform for Gaseous/Liquid Environment." Journal of Microelectromechanical Systems 17 (2008): 483-93.

Synthesis and Characterization of Multifunctional Magnetic Nanoparticles for Treatment of Cystic Fibrosis

Adam Jakus

Materials Science and Engineering, Georgia Institute of Technology

NNIN REU Site: Nanoscience @ UNM, University of New Mexico, Albuquerque, NM

NNIN REU Principal Investigator(s): Marek Osinski, Electrical and Computer Engineering, Computer Science, Physics and Astronomy, University of New Mexico

NNIN REU Mentor(s): Tosifa Memon, Biochemistry, University of New Mexico; Krishnaprasad Sankar, Electrical Engineering, University of New Mexico

Contact: adamjakus@gatech.edu, osinski@chtm.unm.edu, tmemon@unm.edu, krishna@unm.edu

Introduction:

Cystic fibrosis is an inborn genetic disorder that results in a defective transmembrane regulator protein. As a result, the salt concentration within the body's various systems cannot be adequately controlled, producing excess sweat as well as excess viscous mucus in the pancreas, liver, intestines, and lungs that cannot be expelled through by the body's usual processes. Current treatments for infections of the lungs resulting from the stagnant environment are not effective. As a consequence, most individuals with cystic fibrosis die from infections of *Pneumonia aeruginosa* that could normally be treated using antibiotics, but because of the thick mucus barriers, these drugs cannot be efficiently delivered to the sites of infection.

A new method is required to facilitate the transport of antibiotics through the thick mucus. One potential method, and the subject of this work, is to conjugate antibiotic molecules to iron oxide nanoparticles that display super-paramagnetic properties. These nanoparticles could then be directed through the lungs to the regions of infection by applying a direct magnetic field, while simultaneously applying a perpendicular, high frequency alternating magnetic field to induce vibrations causing localized heating, thereby easing the transport of the particles through the mucus. This work focuses on the synthesis of magnetic nanoparticles, their hydrophilization and multifunctionalization with ZnS, fluorescent CdSe quantum dots, and an additional layer of ZnS to allow for easy optical characterization of the dynamic properties of the particles under the influence of a magnetic field *in vitro*.

Experimental Procedure:

The iron oxide nanoparticles were synthesized according to a procedure outlined in detail by Selvan, et al. [1], using a hyperthermal process under a nitrogen atmosphere resulting in hydrophobic particles. A solution of iron pentacarbonyl and oleic acid was refluxed at 290ºC, contrary to the 200ºC suggested in [1], until it turned black in color, upon which an oxidizer, trimethylamine N-oxide, was added.

The final solution was centrifuged to separate out the nanoparticles. These nanoparticles were suspended in hexane and tested using a small magnet to obtain a qualitative determination of their magnetic character. Hydrophilization of the iron oxide cores was attempted using a reduced form of lipoic acid.

A portion of the hydrophobic iron oxide particles were coated with ZnS/CdSe/ZnS following Du, et al. [2] and previous work completed in Dr. Marek Osinski's lab [3]. The particles were injected into a solution of trioctylphosphine oxide and hexadecyl amine under nitrogen prior to injection of zinc and sulfur precursors. Separate solutions of zinc and sulfur precursors were prepared and injected into the hot iron oxide solution in equal volume increments sequentially and allowed to react. Additional zinc sulfide (ZnS) layers were added by performing more injections; typically three ZnS layers were used to cap the iron oxide particles.

A cadmium selenide (CdSe) layer was added to add optical functionality to the particles. This layer was synthesized by first producing a precursor solution of cadmium acetate and selenium in trioctylphosphine. This precursor solution was allowed to interact with the iron oxide/ZnS nanoparticles at elevated temperatures. Upon completion of the reaction, additional capping layers of ZnS were added on top of the CdSe, using the same procedure as previously described.

Results and Discussion:

Iron oxide nanocrystals without (Figure 1) and with (Figure 2) ZnS coating were imaged using a transmission election microscope. From the tunneling electron microscopy (TEM) images, it is apparent that the iron oxide nanoparticles are highly monodisperse at ~ 2-3 nm. These results were produced several times over, indicating reproducibility. Upon addition of the ZnS capping layers, the diameter of the particles increased

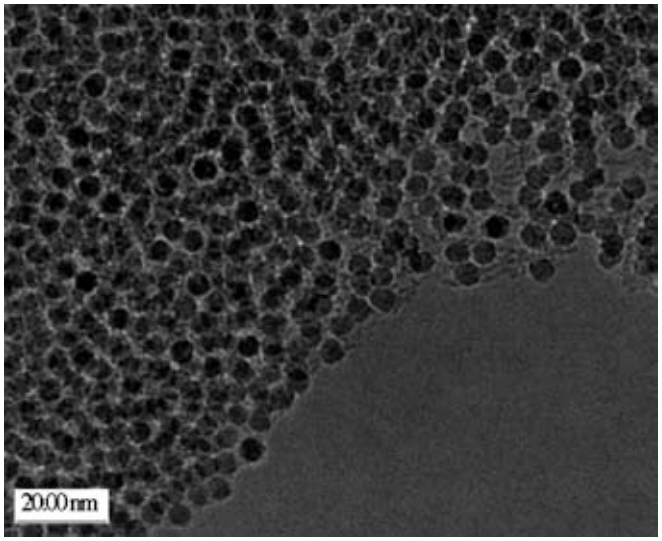

Figure 1: TEM image of iron oxide nanoparticles.

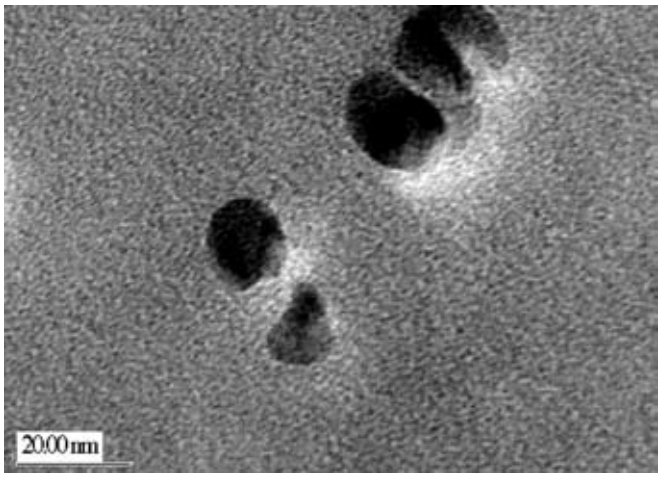

Figure 2: TEM image of ZnS capped iron oxide nanoparticles.

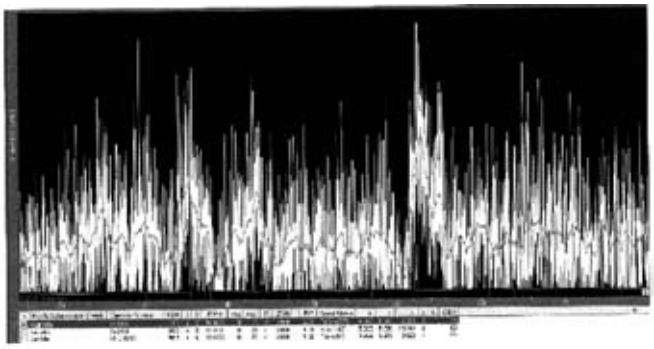

Figure 3: X-ray diffraction profile of iron oxide nanoparticles.

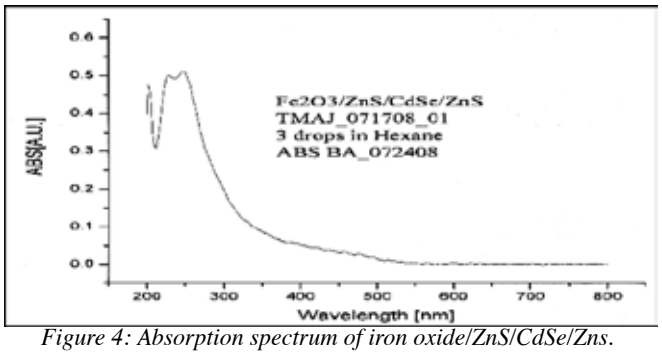

Figure 4: Absorption spectrum of iron oxide/ZnS/CdSe/Zns.

to ~ 10-12 nm. X-ray diffraction (Figure 3) indicates that the iron oxide particles are a mixture of maghemite and magnetite. Although the synthesis outlined by [1] was aimed at producing maghemite, the mixture of species has no negative impact on the magnetic character of the particles as both have inherent superparamagnetic properties at the nanoscale.

Synthesis of the multifunctional iron oxide/ZnS/CdSe/ZnS was unsuccessful. Their magnetic character was minimal, and their absorbance spectrum (Figure 4), indicates limited to no optical excitation, which would be present if the quantum dots were synthesized correctly. From TEM images (not shown), it appears that the CdSe particles were too large to fluoresce and effectively coat the smaller iron oxide/ZnS particles.

The success of the hydrophilization attempts of the iron oxide with reduced lipoic acid is unknown. The necessary equipment required to successfully centrifuge out the small quantity of altered nanocrystals was not present and not available in the time permitted for this research.

Conclusions and Future Work:

Although the synthesis of multifunctional nanoparticles was unsuccessful, the reproducibility of highly monodisperse iron oxide cores is a big step in the right direction. These particles showed significant magnetic character, a necessary property for the proposed application. In addition to the success of the synthesis of the cores was their capping with ZnS.

The procedure for multifunctionalization will need to be modified and perfected before characterization can be done investigating the behavior of these particles within a direct and an alternating magnetic field. Additionally, hydrophilization techniques with lipoic acid, or possibly polyethylene glycol, will need to be perfected.

Acknowledgments:

I would like to thank Prof. Marek Osinski, Tosifa Memon, and Krishnaprasad Sankar for their guidance and support of this work. I would also like to thank Stefi Weisburd, Site Coordinator, for all her help.

This work was funded by the National Science Foundation through the National Nanotechnology Infrastructure Network Research Experience for Undergraduates Program at the University of New Mexico.

References:

[1] S.T. Selvan, P.K. Patra, C.Y. Ang, J.Y. Ying, "Synthesis of Silica-Coated Semiconductor and Magnetic Quantum Dots and Their Use in the Imaging of Live Cells," Angew Chem. Int. Ed. , vol. 46, no. 14, pp. 2448-2452, 2007.

[2] G.H. Du, Z.L .Liu, Q.H. Lu, et al., "Fe3O4/CdSe/ZnS Magnetic Fluorescent Bifunctional Nanocomposites," Nanotechnology, vol. 17, no. 12, pp. 2850-2854, 2006.

[3] Melisa Greenberg and Shin Bowers, "Procedure for CdSe Colloidal Nanocrystal with ZnS Coating Synthesis."

Nano and Microfluidics for Single Molecule Biophysics Applications

Patrick Jurney

Mechanical Engineering, University of Portland

NNIN REU Site: Nanoscience @ UNM, University of New Mexico, Albuquerque, NM

NNIN REU Principal Investigator(s): Dr. Steven Koch, Center for High Technology Materials, University of New Mexico

NNIN REU Mentor(s): Lawrence Herskowitz, Center for High Technology Materials, University of New Mexico

Contact: jurney09@up.edu, sjkoch@unm.edu, lherskow@unm.edu

Abstract:

The recently developed abilities to manipulate and visualize single deoxyribonucleic acid (DNA) molecules are making a significant impact on discoveries in cellular and molecular biology. Innovations in micro- and nanofluidics are an important enabler of single-molecule techniques. Two projects were pursued, one to develop microfluidic devices for optical tweezers applications and one to develop porous nanochannel devices for elongation of single DNA molecules. First, microchannel devices were fabricated using polydimethylsiloxane (PDMS) cured on microfabricated silicon templates for future use with optical tweezers in DNA unzipping applications. The ability to form single-molecule DNA-microsphere tethers was demonstrated. Second, porous-wall nanochannels were fabricated using interferometric lithography and silica nanoparticles for use in visualizing fluorescently labeled DNA molecules. The ability to elongate and visualize lambda phage DNA molecules was confirmed in nanochannels on both silicon and quartz substrates. Both of these achievements are an important foundation for future work in analysis of protein-DNA interactions, including a specific goal of analyzing single chromatin fibers isolated from living cells.

Purpose:

With DNA tethers in microchannels, an optical tweezers apparatus can be used to "unzip" the DNA constructs and ultimately to map where nucleosomes occur on chromatin in living cells by comparing force profiles with thermodynamically predictable controls. While very powerful, the current method of Chromatin Immunoprecipitation (ChIP) and real-time polymerase chain reaction (PCR) has problems with sensitivity and other drawbacks. With mapping by single-molecule unzipping, the accuracy would be improved to approximately three base pairs compared to about 100 base pair accuracy with the current method and will reveal correlations on single molecules [1]. Mapping where nucleosomes occur on chromatin in living cells may also be achievable by labeling histones with either gold nanoparticles or quantum dots and elongating them in nanochannels.

Experimental Procedure:

Photolithography techniques were employed for the fabrication of both the microchannels and the porous nanochannels. The microchannels were first designed using AutoCAD and a mask was printed using an inkjet printer (CAD/Art Services Inc, Bandon, OR). SU-8 2025 photoresist (Microchem Corp, Newton, MA) was then spin coated onto a silicon wafer, exposed, and developed. PDMS (Microchem Corp.) was then mixed with a curing agent and poured over the wafer to create the desired patterns. Finally the PDMS was cut from the template and attached to a glass cover-slide using plasma surface activation. Fluid could then be pumped through the channels either by a syringe pump or, more crudely, syringes, in order to create the desired tethers.

Porous nanochannel fabrication involved bottom-up self-assembly and top-down pattern definition. An anti-reflective coating or ARC was spin coated onto a quartz or silicon substrate followed by photoresist. Interferometric lithography was then used to exposed the chip in a periodic fashion, the exposed chip was then developed creating a template around which the silica nanoparticles were applied using several spin coatings (Figure 1). High temperature calcination was then used to remove the photoresist and enhance the structural stability of the nanoparticle assembly by strengthening the binding between adjacent particles [2]. Lambda DNA (New England BioLabs, Ipswich, MA) stained with YOYO-1 (Invitrogen, Carlsbad, CA) was then placed in the channels and visualized.

Results:

We have familiarized two effective methods of enabling chromatin mapping and general single molecule biophysics research. DNA constructs were assembled in PDMS microchannels. The ability to form tethers was confirmed by observation of microspheres undergoing constrained Brownian motion. Lambda DNA stained with YOYO-1 was visualized in the porous nanochannels using both silicon and quartz substrates (Figure 2).

Conclusions and Future Work:

This work has been an effective enabler of numerous biophysics applications. The most immediate work is attaching thinner PDMS segments to the glass cover-slides so that optical tweezing may be effectively performed without too much scattering. With respect to the nanochannels; attaching PDMS and automating the flow process so that single DNA molecules can be elongated and visualized in about thirty seconds would be a huge accomplishment. Labeling nucleosomes in chromatin extracted from yeast cells with gold nanoparticles or quantum dots and elongating them in these nanochannels is also a priority.

Acknowledgements:

A special thank you is extended to Dr. Steve Koch, my mentor Larry Herskowitz, Anthony Salvagno and the entirety of the Koch Lab along with Deying Xia and the Brueck lab. I would also like to thank Nick Carroll and the Lopez lab for facilitating the use of the Keck Nanofluidics Laboratory, the Center for High Technology Materials, the University of New Mexico, the National Science Foundation, and the National Nanotechnology Infrastructure Network Research Experience for Undergraduates (NNIN REU) Program for their support of my summer in the land of enchantment.

References:

[1] Koch, S. J., A. Shundrovsky, B. C. Jantzen, and M. D. Wang. Probing protein-DNA interactions by unzipping a single DNA double helix. Biophys J 83:1098-1105 (2002).

[2] Deying Xia, Thomas C. Gamble, Edgar A. Mendoza, Steven J. Koch, Xiang He, Gabriel P. Lopez, and S. R. J. Brueck. DNA Transport in Hierarchically-Structured Colloidal-Nanoparticle Porous-Wall Nanochannels (2008).

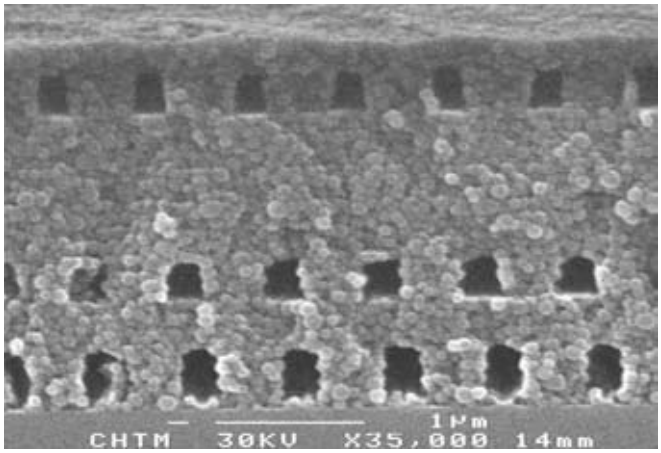

Figure 1: Edge on view of silica nanochannels after calcination demonstrating localized sintering and structural stability (1).

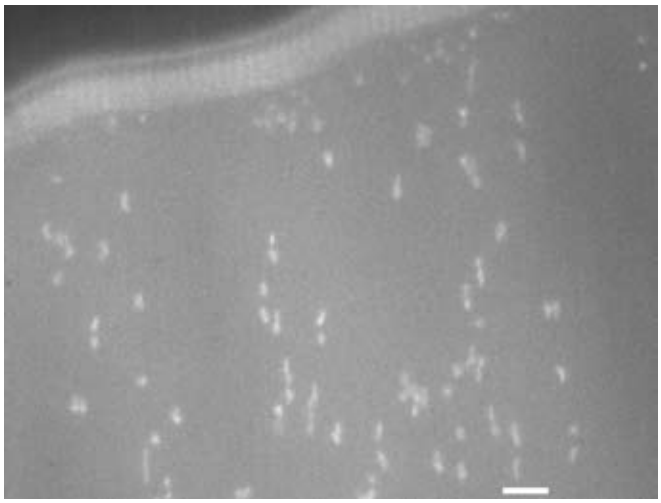

Figure 2: Lambda DNA (bright white streaks) elongated in nanochannels. Scale bar = 5 microns.

Fluorescent Silver Nanoclusters Self-Assembled on DNA

Kishore Padmaraju

Physics, University of Rochester

NNIN REU Site: Nanotech @ UCSB, University of California, Santa Barbara, CA

NNIN REU Principal Investigator(s): Dr. Deborah Fygenson, Physics, University of California, Santa Barbara

NNIN REU Mentor(s): Patrick O'Neill, Physics, University of California, Santa Barbara

Contact: kishore.padmaraju@rochester.edu, deborah@physics.ucsb.edu, patrick@physics.ucsb.edu

Introduction:

Fluorescent chemical groups, known as fluorophores, are essential to fields such as biology and medical imaging. Our group has been investigating a completely new class of fluorophores: silver nanoclusters self-assembled on deoxyribonucleic acid (DNA). These fluorophores are especially interesting because simple changes to their DNA sequence or structure can effectively tune their spectral properties. We are trying to resolve just how sequence and structure influence spectra by investigating and characterizing these fluorescent nanoclusters.

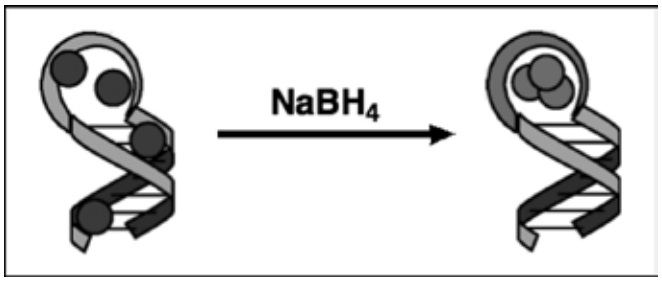

Figure 1: Synthesis of Ag nanocluster.

Synthesis:

Fluorescent silver nanoclusters are hosted in loops comprised of a single strand of DNA bases, also known as hairpins. To synthesize the nanoclusters, we prepare 25 μM of the DNA strand in a solution of 50-500 μM free Ag ions. Adding 25-325 μM $NaBH_4$, a reducing agent, enables the formation of Ag clusters in the hairpins of the DNA (Figure 1).

The synthesis typically produces two or three species of fluorescent nanoclusters, differentiated by their excitation and emission wavelengths. The DNA strand determines which species of fluorescent nanoclusters are produced. Ag and $NaBH_4$ concentrations, as well as the temperature and pH of the solution, determine the proportions of the different nanoclusters.

Experimental Design:

We used fluorescence spectroscopy to characterize the fluorescence of the nanoclusters. Using a fluorimeter, we performed emission scans at incremented excitation wavelengths. From these emission scans we can identify the peak excitation and emission wavelengths of the fluorescent nanoclusters.

We also used mass spectrometry to determine the distribution of cluster sizes in the hairpins. In order to distinguish fluorescent clusters from non-fluorescent clusters at least two sets of data are needed. We identify the fluorescent clusters by correlating a shift in the relative intensity of emitters with a shift in the cluster distribution. To determine the size of the fluorescent clusters we vary the synthesis conditions, often the Ag concentration.

Hairpin loops composed of strictly cytosine bases are the most effective at generating fluorescent nanoclusters. Previous work in this group investigated the 9-cytosine hairpin (9C hairpin). The 9C hairpin hosts a green emitter and a red emitter with emission wavelengths 530 nm and 650 nm, respectively. Fluorescence spectroscopy and mass spectrometry identified the Ag_{11} cluster as the green emitter and the $Ag_{13\text{-}15}$ clusters as red emitters.

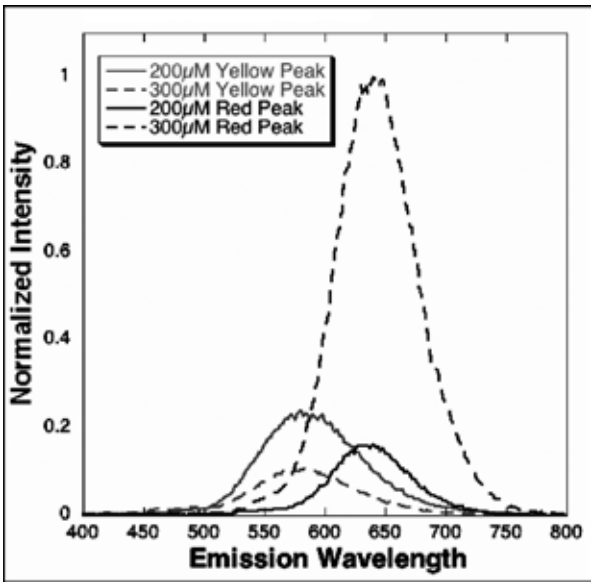

Figure 2: Emission scans of 12C hairpin.

Our research investigated nanoclusters hosted in 12C hairpins. The 12C hairpin hosts a yellow emitter with emission wavelength 580 nm and a red emitter with emission wavelength 650 nm. The red emitters of the 9C and 12C hairpins have the same excitation and emission wavelengths. Our goal was to determine whether the size of the 12C's red emitter was the same size as that of the 9C hairpin. Confirmation would support the hypothesis that the number of Ag atoms comprising the nanocluster is a major determinant of its spectral characteristics.

Results and Conclusions:

With the 12C hairpin, we found that lower concentrations of Ag during synthesis favored the yellow emitter and that higher concentrations of Ag favored the red emitter. Figure 2 depicts normalized emission scans of the red and yellow fluorescence for Ag concentrations of 200 μM and 300 μM. Given the low concentration of emitters in these solutions, we expect a linear relationship between the fluorescence and the number of emitters. Increasing the Ag concentration from 200 μM to 300 μM decreases the number of yellow emitters by a factor of two and increases the number of red emitters by a factor of five.

The cluster size distribution in Figure 3 displays a broad shift in cluster sizes between samples. By contrast with previous work on the 9C hairpin, where specific clusters were identified as emitters, we can only establish ranges of 3-7 atom clusters for the yellow emitter and clusters of 13 atoms or more for the red emitter. We attempted to identify the emitter sizes using selective photobleaching, that is, exposing the sample to intense light that had been filtered to contain only the excitation light of one of the emitters. Due to the limited photostability of these fluorophores, we expected the excited emitter to stop fluorescing and the non-excited emitter to retain its fluorescence. We exposed the nanoclusters for 5 minutes to a mercury lamp filtered to excite only the red emitter. The fluorescence of the yellow emitter was preserved while the fluorescence of the red emitter was diminished by a factor of three. However, the mass spec spectra of two samples showed no difference in distribution of cluster sizes, prohibiting the identification of fluorescent emitters and indicating that the cluster fluorescence is more strongly determined by factors other than cluster size.

Focusing on the yellow emitter of the 12C hairpin, we analyzed a different strand that hosted the same yellow emitter, the 6C dumbbell. The 6C dumbbell consists of a duplex with a 6C hairpin on both ends. Fluorescence of the 6C dumbbell has a temperature sensitivity that we were able to exploit. When a sample, originally synthesized in refrigerated conditions, was incubated for 15 hours at 35°C, the number of yellow emitters decreased by a factor of 1.5 and the number of red emitters increased by a factor of 5. Surprisingly though, the mass spec, shown in Figure 4, again indicates no change in the cluster distribution between samples.

The ranges of cluster sizes established for the emitters are consistent with the hypothesis that the number of Ag atoms determines nanocluster fluorescence. However, our photobleaching and incubation experiments suggest that cluster fluorescence is determined not only by the number of Ag atoms, but also by features such as cluster geometry, cluster charge, or specific Ag-DNA bonds as well. Our work has been instrumental in helping this group determine to redirect further research on these fluorophores towards such features.

Acknowledgments:

I would like to thank my mentor Patrick O'Neill and Dr. Deborah Fygenson for the time and resources they dedicated throughout my research experience. I would also like to thank the Fygenson group for their input, as well as the National Nanotechnology Infrastructure Network Research Experience for Research Program and National Science Foundation.

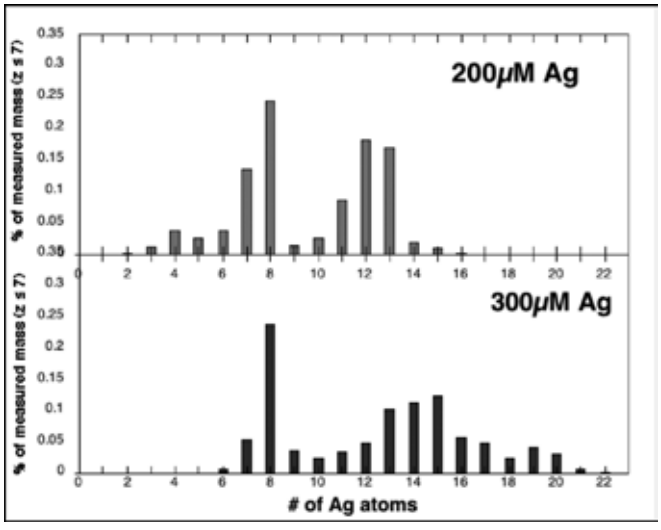

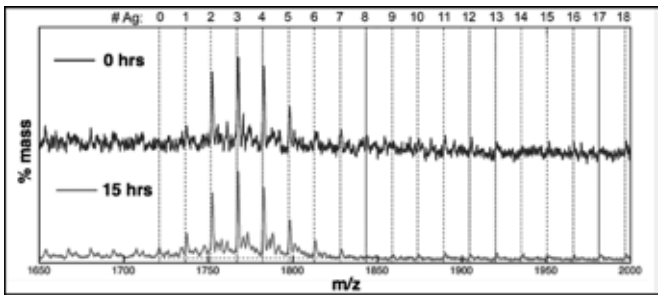

Figure 3, left: Cluster distribution of 12C hairpin.

Figure 4, above: Mass spec of 6C dumbbell.

A Wireless Remote Biosensor for the Detection of Biological Agents

Taemee Pak

Chemical Biology, Stony Brook University

NNIN REU Site: Cornell NanoScale Science and Technology Facility, Cornell University, Ithaca, NY
NNIN REU Principal Investigator(s): Dr. Carl Batt, Food Science, Cornell University
NNIN REU Mentor(s): Matthew Kennedy, Electrical and Computer Engineering, Cornell University
Other Contributors/Mentors: Scott Stelick, Clarissa Lui, Diego Rey; Cornell University
Contact: tpak@ic.sunysb.edu, cab10@cornell.edu, mjk67@cornell.edu

Abstract:

A biosensor capable of wireless data transfer has been designed, fabricated, and tested. The sensor uses aptamers immobilized to a pair of interdigitated electrodes to detect *Staphylococcus enterotoxin B* (SEB). We have designed a solvent-free method to fabricate sensor chips comprised of interdigitated gold electrodes (150 nm thickness) evaporated onto a silicon substrate. The electrodes are functionalized with thiol-modified aptamers that were chosen based upon their bioaffinity for the target analyte. Upon contact with SEB, discriminative binding between SEB and electrode-bound aptamers occurs thereby producing an observable change in the electrical properties of the electrodes. A minimum two-fold increase in capacitance resulted from sensor exposure to SEB in comparison to exposure to non-specific proteins, thereby demonstrating device sensitivity and selectivity for the target analyte. Ultimately, we envision that this device may be used for remote detection of biological agents, thereby limiting the exposure of humans to potential biological threats.

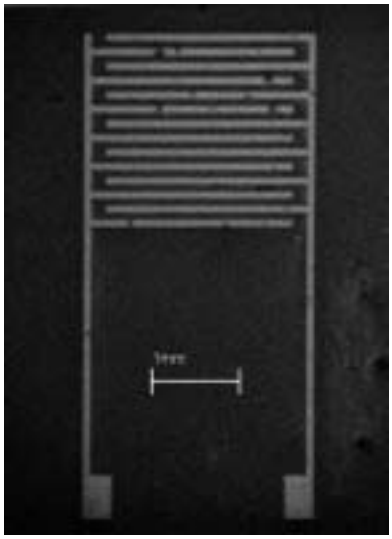

Figure 1: SEM of gold interdigitated electrodes with 100 μm interdigital spacing.

Introduction:

A device with the ability to sensitively and selectively detect target molecules is a technology of interest because of its applications in military and public health sectors. Electronic biosensors may be manufactured at small dimensions with small features while necessitating very low power. They may also be connected to a system consisting of a data acquisition and a base station module that wirelessly transmits data from the sensor to a computer for analysis. Though electronic sensors have shown sensitivity, selectivity has been a persistent issue and has forced current biosensors to rely on optical methods such as surface plasmon resonance and molecular flow cytometry which require on-site illumination and power sources. An electronic biosensor with wireless capabilities will introduce a new generation of nanoscale biosensors.

Experimental Procedure:

Sensor Fabrication. 2 μm of Parylene C were vapor-deposited onto a 100 mm diameter silicon wafer. Two coats of photoresist were spun and soft-baked. Sensor electrodes were UV-patterned onto the wafer before post-exposure baking and development. Oxygen plasma reactive ion etching (RIE) was then employed as a parylene etchant. Electron gun evaporation was used to deposit 10 nm titanium and 150 nm gold on top of the parylene in unexposed areas and on top of Si in exposed areas, the titanium layer facilitating adhesion at the gold-silicon interface. Residual parylene was peeled from the wafer using tweezers. Wafer dicing yielded individual chips that were wire-bonded to copper breadboard circuits. In sensor functionalization, thiol-modified nucleic acid probes with an SEB bioaffinity ("spiegelmers") were used because of their resistivity to natural enzymatic degradation. 20 μL of 50 mM spiegelmer solution were pipetted onto the sensors and incubated for 8 hours at ambient temperatures to ensure spiegelmer immobilization onto the electrodal surface via thiol chemistry (Figure 2).

Electrical Characterization. A wire-bonded sensor chip was connected to a capacitance meter before a baseline reading was taken with phosphate buffer. After 10 minutes of equilibration, the chip was exposed to SEB. Subsequently, the chip was rinsed three times with buffer. A post-wash reading was taken while the sensor was again exposed to buffer. Residual SEB-spiegelmer binding was expected to be reflected in capacitance. The chip was incubated with 20 mM sodium hydroxide (NaOH) for 5 minutes and washed three times with buffer before a final buffer reading was taken. If

the altered capacitance was due to SEB-spiegelmer binding, the post-NaOH reading should return to baseline. The sensor was kept in the dark during characterization because previous results indicated that the sensors are light-sensitive due to photoelectric effects.

Results and Conclusions:

Preliminary electrical characterization showed sensor selectivity towards SEB, reporting nearly a two-fold increase in capacitance upon SEB addition to the sensor relative to the capacitance upon sensor exposure to bovine serum albumin (BSA). Water showed a (262 ± 15)nF capacitance increase from baseline and a (109 ± 15)nF disparity from the BSA control whereas phosphate buffer showed a (298 ± 28)nF capacitance increase and a (188 ± 48)nF disparity. Furthermore, a slightly-elevated capacitance was recorded after an initial wash which dropped back to baseline post-NaOH incubation (Figure 3). This re-occurring capacitance pattern is indicative of SEB-spiegelmer binding. These results were seen in both de-ionized water and 10-μM phosphate buffer, although significant salt-shielding effects were detected as buffer concentration increased possibly because of interactions between salts and nucleic acids at higher concentrations.

Furthermore, upon addition of a protein cocktail containing BSA, green fluorescent protein (GFP), and SEB in water, there was an initial capacitance increase of (288.5 ± 0.5)nF. Upon system stabilization, the capacitance settled at 237-nF whereas the control cocktail (BSA+GFP) showed a 61-nF increase from baseline, a 176-nF disparity (Figure 4). The capacitance returned to baseline post-NaOH incubation, demonstrating SEB selectivity during exposure to protein arrays and proving viability for practical sensing applications.

Voltaic characterization using a wireless system was performed as well; however, the data acquisition module was flawed in design. Nevertheless, the sensors were capable of successful wireless data transfer and preliminary voltaic results showed efficient SEB detection with the characteristically-elevated voltage readings indicative of SEB-spiegelmer binding.

Future Work:

The next steps involve acquiring consistent electrical characterization results with phosphate buffers that have environmentally-relevant salt concentrations and conducting voltaic experiments using the wireless biodetection system upon re-designing of the data acquisition module.

Acknowledgements:

I extend my sincere gratitude to Dr. Carl Batt and the Batt Research Group. I would also like to thank the Cornell NanoScale Science & Technology Facility (CNF), National Nanotechnology Infrastructure Network Research Experience for Undergraduates Program, National Science Foundation (NSF), NYS Center for Advanced Technology, and the Center for Life Sciences Enterprise for funding.

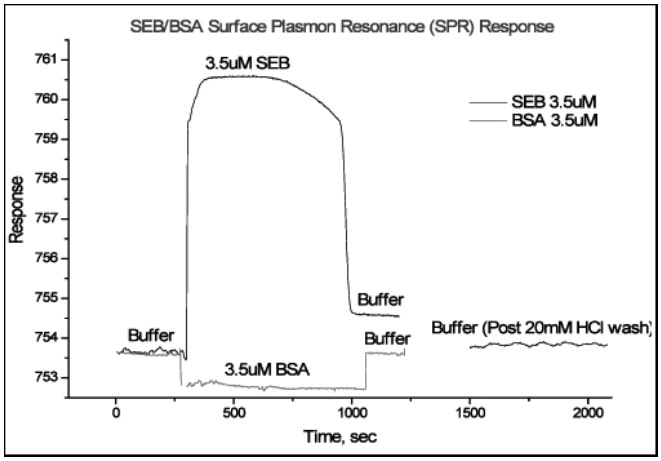

Figure 2: SPR confirmed effective functionalization of electrodes by spiegelmers and spiegelmer functionality.

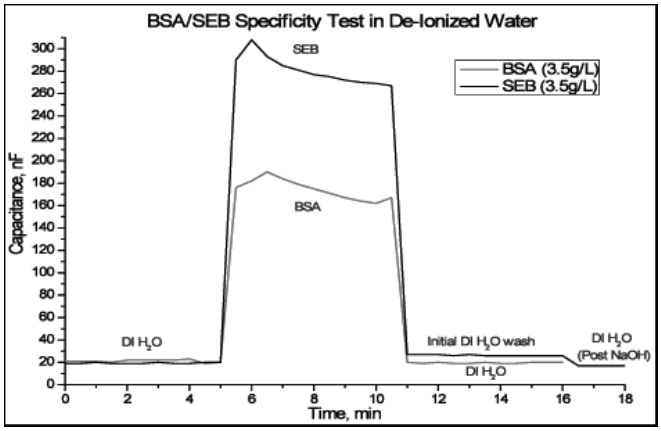

Figure 3: Specificity assays. There is a two-fold capacitance increase upon sensor exposure to SEB with elevated post-wash capacitance.

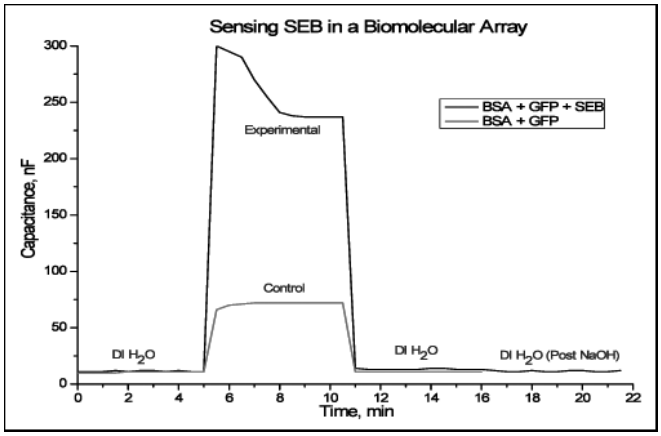

Figure 4: Selectivity assay. The BSA+GFP+SEB capacitance response was four times greater than the BSA+GFP capacitance response, demonstrating sensor selectivity for SEB.

Nano Meets Micro: Synthesis of Proteins for the Organization of Nanostructures

Laurel Schmidt

Undeclared, Carleton College

NNIN REU Site: Center for Nanotechnology, University of Washington, Seattle, WA

NNIN REU Principal Investigator(s): Dr. Beth Traxler, Microbiology, University of Washington

NNIN REU Mentor(s): Ruth Hall, Microbiology, University of Washington

Contact: schmidtl@carleton.edu, btraxler@u.washington.edu, rah7@u.washington.edu

Abstract:

Manufacturing reliable nanoelectronics can be challenging, simply because of the scale on which these devices are built. In the future, it may be effective to find a way to direct their self-assembly. Certain proteins can be genetically engineered to assist in this process. Permissive sites, which allow for the insertion of short amino acid sequences without a loss of function, have been identified in two different proteins from the bacterium *Escherichia coli*, LacI and TraI. A short polypeptide sequence with a known affinity for silver particles was inserted into different permissive sites in each protein, and the resulting modified proteins were characterized. LacI derivatives successfully repressed expression of β-galactosidase, an enzyme whose transcription is controlled by LacI. TraI derivatives participated successfully in conjugation. An assay was attempted to measure the proteins' affinity for silver, but the results were inconclusive; a different assay will be needed in the future. The expected ability of these modified proteins to bind strongly to both deoxyribonucleic acid (DNA) and inorganic particles suggests they could play a key role in the organization of nanostructures by arranging silver particles in defined patterns along a DNA template.

Introduction:

The broad goal of this project is to create a library of proteins that can bind to both DNA and inorganic particles. These proteins can be used to determine where in a cell a certain protein is most concentrated, or to organize nanoparticles along a DNA scaffold, perhaps leading to self-assembling structures with applications in nano- electronics and -photonics. Researchers have had success modifying proteins to bind to several inorganics; this work builds on their work by modifying two proteins to bind to silver.

Many proteins made by the bacterium *E. coli* naturally have the ability to bind to DNA. Researchers have already identified permissive sites in several of these, including LacI and TraI. LacI is a transcriptional repressor: when there is no lactose present in a cell, LacI binds to dsDNA at the operator sequence and prevents the transcription of the genes that follow. These genes encode the enzyme β-galactosidase which breaks down lactose. If lactose is present in the cell, LacI releases, and the genes are transcribed.

TraI is involved in F-plasmid conjugation, the process by which bacteria transfer DNA to one another. TraI binds to a double-stranded DNA plasmid in the donor bacterium and nicks it, and then helps it unwind so that one strand can be transferred to the recipient. Both bacteria then synthesize the complementary strand of DNA. While LacI binds only at its 30 base dsDNA operator sequence, TraI has the ability to bind non-specifically on both ds and ssDNA. Different applications in the future may require sequence-specific or sequence-independent binding, so both proteins were used.

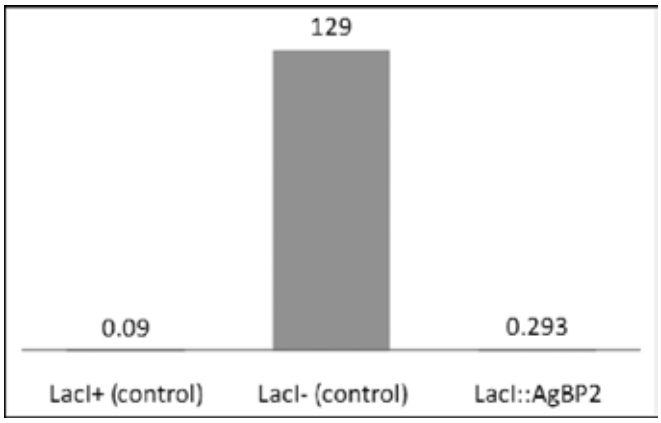

Figure 1: Level of β-galactosidase activity for cells carrying three different versions of LacI

Using a phage display system, researchers have identified a cysteine-constrained 12 amino acid peptide (EQLGVRKELRGV), known as AgBP2, with a high affinity for silver. This sequence was inserted into the permissive sites of LacI and TraI after the 317th and 369th amino acids, respectively, to produce LacI::AgBP2 and TraI::AgBP2. These derivatives were identified using polymerase chain reaction (PCR) screening, DNA sequencing, and expression samples, and then characterized for their affinities to DNA and silver.

Characterizing DNA-Binding:

Since LacI represses synthesis of β-galactosidase, a high level of DNA binding by LacI::AgBP2 would be associated with a low level of • β-galactosidase activity. Figure 1 shows the level of β-galactosidase activity for cells carrying three different versions of LacI; the units shown in the chart are proportional to the level of β-galactosidase activity per cell per unit time. The LacI::AgBP2 showed wild type-level β-galactosidase repression.

Because the ability of TraI to bind to DNA is necessary for conjugation, a mating assay was performed to characterize TraI::AgBP2 DNA-binding activity. TraI::AgBP2 had wild type-level mating activity.

Characterizing Silver-Binding:

To determine the affinity of LacI::AgBP2 and TraI::AgBP2 for silver, clarified cell extracts were mixed with silver powder. After suspension and centrifugation, the supernatant was saved, and the powder was washed twice and then resuspended. Ideally, proteins exhibiting no binding would be found in the initial supernatant, those showing nonspecific binding would come off in one of the washes, and those with a strong affinity for silver would remain with the powder until the end. However, as shown in Figure 2, the affinity of modified proteins for silver was not demonstrated to be any stronger than that of the unmodified proteins. This particular method of measuring binding ability had sometimes been ineffective in the past, and the silver nanoparticles agglomerated into larger particles during the pre-test preparation phase, indicating that this test for Ag binding is not accurate. Future characterization will assess binding on Ag surfaces with purified proteins.

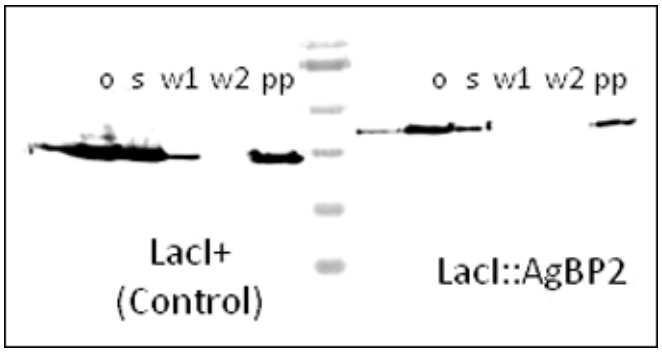

Figure 2: Results of silver binding assay. o = original amount of protein; s = supernatant; w1 = wash 1; w2 = wash 2; pp = powder pellet.

Conclusions and Future Work:

Derivatives of LacI and TraI containing a silver-binding peptide have been synthesized successfully, and their sequences have been confirmed. LacI::AgBP2 shows wild type-level β-galactosidase repression, verifying its *in vivo* binding to DNA at the *lac* operator. TraI::AgBP2 exhibits wild type-level mating activity, indicating wild type-level DNA binding. The abilities of both derivatives to bind to silver have not been demonstrated. To further characterize these proteins, a more accurate and quantitative assay is needed. Surface plasmon resonance or quartz crystal microbalance will be used to characterize silver binding. Silver and DNA binding will be visualized via atomic force or electron microscopy. Such images could confirm ability of the proteins to bind to silver and DNA simultaneously, and perhaps demonstrate the expected sequence-specific binding of LacI derivatives and sequence-independent binding of TraI derivatives.

Acknowledgements:

I would like to thank my PI, Dr. Beth Traxler, my mentor, Ruth Hall, my lab mates Eli Gachelet and Rembrandt Haft, and my site coordinator Ethan Allen for guidance and encouragement. I would like to thank the National Nanotechnology Infrastructure Network Research Experience for Undergraduates Program and the National Science Foundation for funding.

Direct-Fabrication of Nanoparticles in Cancer Diagnostics

Trisha Sengupta

Biology, Emory University

NNIN REU Site: Stanford Nanofabrication Facility, Stanford University, Stanford, CA

NNIN REU Principal Investigator(s): Dr. Yi Cui, Materials Science and Engineering, Stanford; Dr. Mary Tang, Stanford Nanofabrication Facility, Stanford University

NNIN REU Mentor(s): Ching-Mei Hsu, MSE; Stephen Connor, Chemistry; Stanford University

Contact: tsengup@emory.edu, chingmei@stanford.edu, stconnor@stanford.edu, yicui@stanford.edu, mtang@stanford.edu

Abstract:

Synthetic antiferromagnetic (SAF) nanoparticles possess unique tunable magnetic properties, which make them instrumental in developing highly selective, highly sensitive bioassays for tumor detection and surveillance. Through a combination of top-down and bottom-up approaches, we are able to fabricate these nanoparticles and bypass the disadvantages of following either single approach. Monodisperse SAF nanoparticles are fabricated by means of nanoimprint lithography (NIL), a top-down process. However, the method we used to construct the template of nanopillars for NIL mainly involved the bottom-up approach, which involved the following steps; synthesis of silica nanoparticles, surface functionalization, deposition by Langmuir Blodgettry, and reactive ion etching. Scanning electron microscope (SEM) images after the etching step show that we were able to construct uniform arrays of nanopillars on a silicon wafer, thus resulting in a low-cost and production-worthy stamps for fabricating SAF nanoparticles.

Introduction:

Magnetic nanoparticles show great promise in improving medical diagnostics, treatments, and therapies due to their relatively small size in comparison to biomolecules, and their externally controlled magnetization. Particularly, magnetic nanoparticles have made significant advances in bioanalysis. In our case, the ultimate goal was to improve the process of magnetic sorting for a multiplexed bioassay [1].

This process involves a deoxyribonucleic acid (DNA) probe, which is bound to a biosensor, to hybridize with a complementary strand which is attached to a magnetic nanoparticle. The biosensor is able to detect magnetization, and therefore quantify the amount of the target DNA [2].

Our objective was to fabricate stamps for nanoimprint lithography (NIL). The stamps were fabricated according to the following steps; synthesis of silica nanoparticles, surface functionalization, deposition by Langmuir Blodgettry (LB), and reactive ion etching (RIE)—as depicted in Figure 1. Once the stamps were made, they were used in a top-down process, which involved a combination of nanoimprint lithography (NIL) and lift-off to produce SAF nanoparticles. Our group has previously demonstrated the use of LB to produce stamps and used those stamps to produce templates for SAF nanoparticle fabrication. However, the complete process to use these stamps and templates to produce the SAF nanoparticles has not yet been completed. Here, we were fabricating stamps which would be utilized in this process, so that the SAF nanoparticles could be fabricated and investigated as bioassays for cancer.

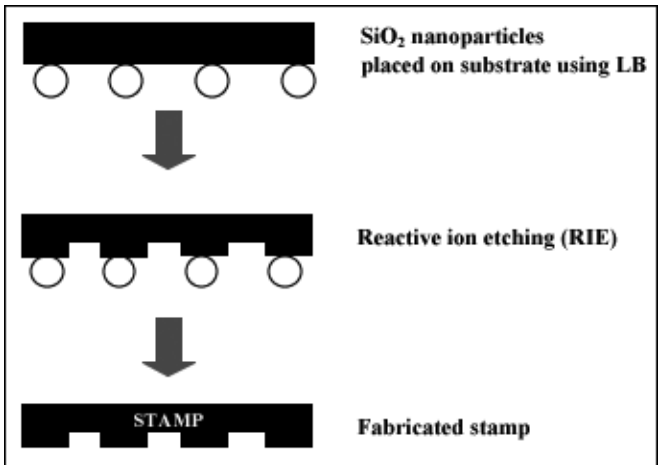

Figure 1: Fabrication of stamp for NIL and liftoff.

Herein, we report on the reactive ion etching (RIE) of the SiO_2 mask to produce stamps. The etching requires a two-step process; shrinking the SiO_2 nanoparticles, and anisotropic etching to form a stamp of uniformly distributed nanopillars.

Experimental Procedure:

The LB method was applied to pattern an etch mask. Afterwards, a reactive ion etch (RIE) was performed on the etch mask in order to obtain a nanopillar array with straight sidewalls. By using an isotropic etch with a fluorine-based

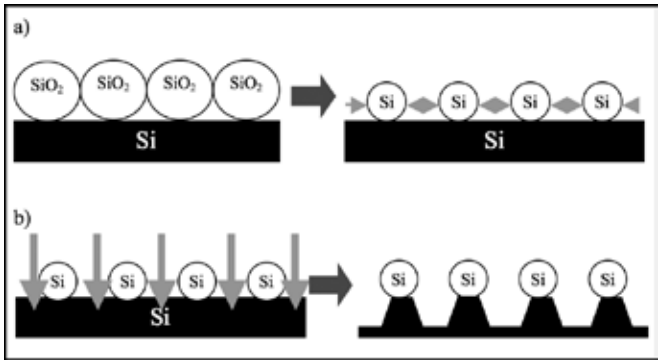

Figure 2: a) Isotropic etching of SiO_2 mask with fluorine-based etchant; b) Anistropic etching of Si with $O_2/Cl_2/HBr$.

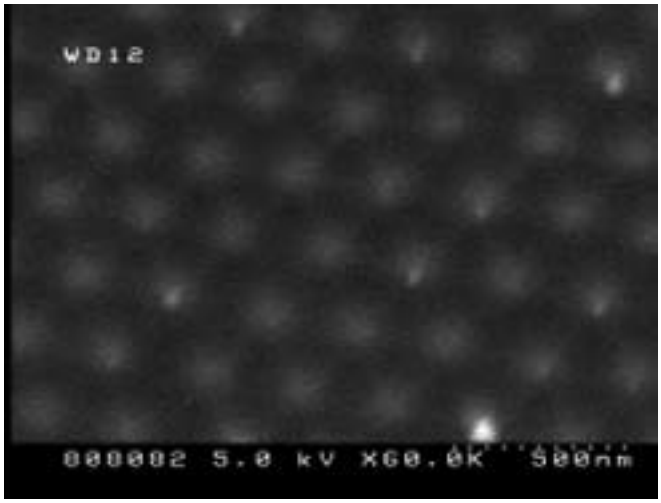

Figure 3: Planar SEM view of nanopillars of stamp.

etchant, we shrank the mask of SiO_2 nanoparticles, and then we used a combination of $O_2/Cl_2/HBr$ to achieve anisotropic etching as demonstrated in Figure 2. However, scattering caused the sidewalls to be slightly sloped. Additionally, mask erosion was caused by imperfect selectivity and physical etching. Scanning electron microscopy (SEM) was used to characterize the pillars.

Results and Conclusion:

We obtained the expected result after RIE, which were sloped nanopillars. The slight sloping might be caused by scattering as shown in Figure 3. After plasma etching the 250 nm SiO_2 nanoparticle mask, the resulting nanopillars were approximately 120 to 150 nm in diameter. Using Langmuir Blodgett, the uniformity of the size and distribution of the SiO_2 nanoparticles allowed for the etching to be uniform. Conversely, the etch mask created using spin-coated latex-spheres possessed microdomains, and after RIE, the different etching rates in and out of those domains produced an unevenly distributed and sized nanopillar stamp. Therefore the template for SAF nanoparticle fabrication produced using this technique will also be uniform in distribution and size, while the latex-sphere technique has not be uniform.

Ultimately, the stamps were fabricated for a nanoimprinting process to produce SAF nanoparticles for cancer detection. We successfully utilized a two-step etch process to create the stamp.

Future Work:

Our future plans involve ion milling the stamp to round out the pillars and ensure that the liftoff does not remove the magnetic material in the troughs. These stamps will then be used to produce SAF nanoparticles for cancer bioassay. Additionally, we can utilize the uniformity created by this general stamp fabrication technique for microfluidics and optics. The stamp may also be used as a template for other nanomaterial growth.

Acknowledgments:

I would like to thank Dr. Michael Deal, Mingliang Zhang, Ben Weil, James Conwayk, SNF Process Staff, Mihir Tendulkar, and Maureen Baran for making my research possible. This work was supported by the Stanford Nanofabrication Facility, Centers of Cancer Nanotechnology Excellence, NSF, and the National Nanotechnology Infrastructure Network Research Experience for Undergraduates (NNIN REU) Program.

References:

[1] Wei Hu, Robert J. Wilson, AiLeen Koh, Aihua Fu, Anthony Z. Faranesh, Christopher M. Earhart, Sebastian J. Osterfeld, Shu-Jen Han, Liang Xu, Samira Guccione, Robert Sinclair, Shan X. Wang, High-Moment Antiferromagnetic Nanoparticles with Tunable Magnetic Properties, Advanced Materials, 20 (2008), pp. 1479-1483.

[2] S.X. Wang, S.-Y. Bae, G. Li, S. Sun, R.L. White, J.T. Kemp and C.D. Webb, Towards a magnetic microarray for sensitive diagnostics, J. Magn. Mater. 293 (2005), pp. 731–736.

Cellulose Fibril Patterning for Real Time Studies of Cellulase Kinetics

Rachel Simmons

Biological Engineering, Utah Sate University

NNIN REU Site: Cornell NanoScale Science and Technology Facility, Cornell University, Ithaca, NY

NNIN REU Principal Investigator(s): Larry Walker, Ph.D., Biological and Environmental Engineering, Cornell University; Jose Moran-Mirabal, Ph.D., Biological and Environmental Engineering, Cornell University

Contact: rachel.simmons@aggiemail.usu.edu, lpw1@cornell.edu, jmm248@cornell.edu

Abstract:

Cellulases are key enzymes in the breaking down of cellulose into fermentable sugars used for bioethanol production. Lignocellulose-based biofuels have shown to be a viable alternative to fossil fuels. However effective production of cellulosic bioethanol is dependent on understanding kinetic interactions between cellulases and cellulose. A technique for immobilizing cellulose fibrils on solid substrates using a polymer lift-off method that allows for real time imaging of cellulase-cellulose interactions has been developed.

Photolithographically patterned features on a thin polymer coating allow exposure of selected areas of the solid substrate to the cellulose fibrils. Incubation of the cellulose followed by drying, and subsequent polymer lift-off results in the immobilization of cellulose aggregates and yields specific morphologies depending on the pattern size used for the immobilization. The specific pattern attributes the various patterned features allow for imaging of immobilized cellulose mats, particles, or fibrils. Cellulose and *Thermobifida fusca* cellulases Cel6B and Cel9A can be fluorescently tagged and in combination with cellulose immobilization, can be imaged via fluorescence microscopy. This fluorescence-based system can be used to elucidate interactions between cellulose fibrils and the cellulases involved in depolymerization.

As part of this project, novel patterns containing registration and alignment marks were developed. These patterns can be used to identify specific cellulose features and image them in real time. Furthermore, the registration marks included in the novel patterns allow the tracking of specific cellulose features over prolonged time-lapsed experiments. Immobilization and identification through photolithographic patterning in combination with quantitative fluorescence microscopy techniques will result in a better understanding of cellulose-cellulase interactions. This can provide a more thorough understanding of the steps involved in the depolymerization of cellulose into fermentable sugars, which will aid the formulation of enzyme cocktails that improve the efficiency and reduce the cost of bioethanol.

Introduction:

Cellulases are instrumental in the depolymerization of cellulose fibrils into fermentable sugars for bioethanol production. Development of the most effective cocktail of enzymes for the depolymerization of cellulose fibrils into fermentable sugars is dependent upon understanding the intrinsic molecular mechanisms of cellulases. In turn, the design and creation of effective cellulase cocktails will dramatically reduce the cost of bioethanol production from lignocellulosic biomass.

Techniques that would allow for the evaluation of enzyme performance on insoluble cellulose materials ranging from single fibrils to complex cellulose mats are important for observing on-off rates and processive behaviors of cellulases. Effective imaging of these behaviors mandates high spatial and temporal imaging resolution, and in order to achieve these parameters, cellulose fibrils must be immobilized on a solid substrate.

This project developed a polymer lift-off technique that allowed for cellulose immobilization on a solid substrate by photolithographically patterning an evaporated polymer coating on a glass substrate. The immobilization of cellulose fibrils was achieved by selectively exposing the underlying glass surface and then removing the unpatterned cellulose by lifting off the polymer coating.

Experimental Procedure:

Polymer lift-off surfaces with specific pattern designs for fibril immobilzation were fabricated on 170 μm thick fused-silica wafers ranging in diameter from 15 mm to 54 mm. The wafers were initially cleaned with three successive 10 minute baths in acetone, isopropanol and deionized water, followed by drying under a nitrogen stream. Further removal of organic contaminants was performed by 10 min of oxygen plasma cleaning (60 mTorr, 50 SCCM 0_2, 150W, Oxford PlasmaLab 80+ RIE System). The back sides of the wafers were attached to adhesive tape to protect them from polymer deposition. A 1 μm thick conformal coating of di-para-xylylene (Specialty Coating Systems) was evaporated onto the wafer surfaces, after which the adhesive tape was removed.

Shipley 1827 photoresist was spun over the polymer coating on the wafers to a thickness of 3.5 μm and baked at 90°C for 1 minute. Photolithography was performed using an HTG System IIIHR Contact Aligner. The exposed photoresist was

developed in AZ300-MIF developer (Clariant Corp., AZ Electronic Materials) for 1 min, followed by a 1 min rinse in deionized water and dried under a nitrogen stream.

Exposed regions of the polymer layer were etched in a reactive oxygen ion plasma chamber (60 mTorr, 50 SCCM 0_2, 150W, Oxford PlasmaLab 80+ RIE System). Residual photoresist was removed by successive 10 minute baths in acetone and isopropanol.

Results and Conclusions:

The polymer lift-off technique was successful in immobilizing cellulose fibrils on solid substrates, and allowed for high resolution fluorescence imaging of cellulose-cellulase interactions. Different patterned features yielded varying cellulose aggregate sizes. 10 μm features in width were most effective in immobilizing single cellulose fibrils and small fibril aggregates. 10 μm diameter dots were successful in isolating single cellulose fibrils important for imaging. Features smaller than 10 μm were not consistent in immobilizing cellulose fibrils, as most material was removed in the lift-off process and only small fibrils remained in patterned features. Patterns larger than 10 μm in width yielded larger cellulose aggregates and cellulose mats. Pattern alignment schemes allowed for identification of specific pattern features and cellulose fibrils.

Acknowledgments:

Photolithography was performed at the Cornell NanoScale Facility. The project was supported by the NSF via NNIN REU Program. The project was also supported by the departments of Biological and Environmental Engineering, and Applied Physics and Engineering at Cornell University.

References:

[1] Ilic, B. Topographical Patterning of Chemically Sensitive Biological Materials Using a Polymer-Based Dry Lift Off. Biomedical Microdevices. 2000 2:4, 317-322.

[2] Moran-Mirabal, J. Controlling Microarray Spot Morphology with Polymer Liftoff Arrays. Anal. Chem. 2007, 79, 1109-1114.

[3] Moran-Mirabal, J. Micrometer-Sized Supported Lipid Bilayer Arrays for Bacterial Toxin Binding Studies through Total Internal Reflection Fluorescence Microscopy. Biophysical Journal. 2006, 89, 296-305.

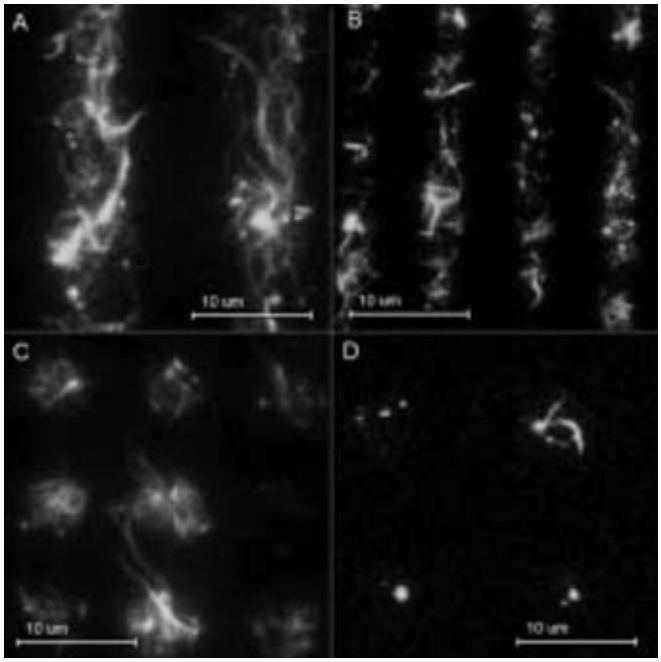

Figure 1: Imaging of immobilized cellulose particles on solid substrate. A) 10 µm wide lines immobilized cellulose agregates and celulose bundles with some single fibrils. B) 5 µm wide lines immobilized single cellulose fibrils and smaller cellulose bundles. C) 10 µm dots immobilized single cellulose fibrils and cellulose bundles. D) 5 µm diameter dots immobilized single fibrils and very few larger bundles.

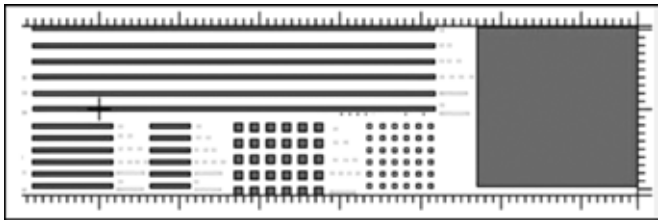

Figure 2, upper middle, right: Solid substrate pattern design with alignment scheme. Different feature sizes (ranging from 5 µm to 500 µm in width) were designed to immobilize various cellulose bundle sizes for imaging.

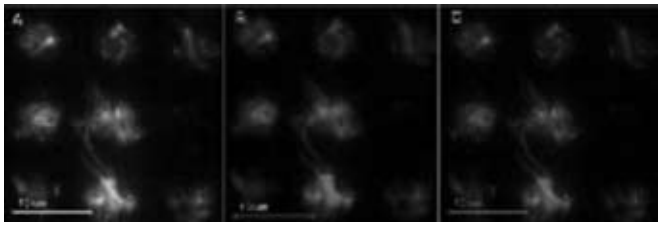

Figure 3, lower middle, right: 10 µm diameter dots incubated with Thermobifida fusca cellulases allowed for imaging of cellulose-cellulase interactions. A) Cellulose incubated with AF488-Cel6B enzyme. B) Cellulose incubated with AF 647-Cel9A enzyme. C) Combined fluorescence of both Cel6B and Cel9A.

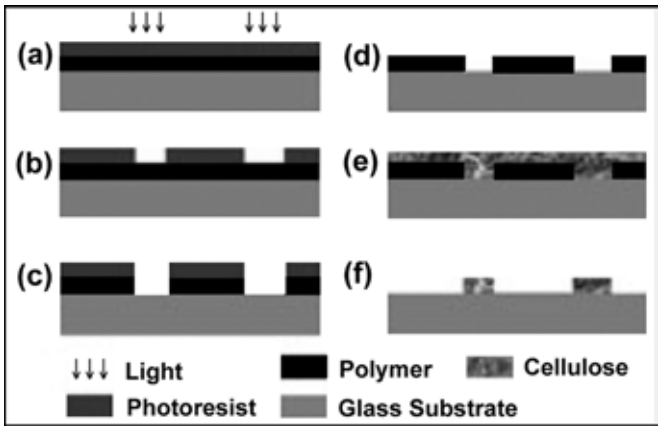

Figure 4, bottom: Surface patterning and cellulose immobilization through polymer lift-off. (a) Glass surface is coated with a thin polymer layer and photoresist is spun on and exposed though a mask. (b) Wafer is developed and exposed photoresist areas are washed away. (c) Exposed polymer is reactive ion etched with oxygen ion plasma, exposing the underlying glass surface. (d) Left over resist is removed. (e) Cellulose in aqueous solution is dried on the patterned surface. (f) Polymer is lifted-off leaving behind cellulose fibrils and fibril bundles in patterned areas.

Fabrication and Optical Characterization of Nanoimprinted Plasmonic Constructs for Biosensor Applications

Isaias Tesfaslassie

Applied Physics, Appalachian State University

NNIN REU Site: Lurie Nanofabrication Facility, University of Michigan, Ann Arbor, MI

NNIN REU Principal Investigator(s): L. Jay Guo, Department of Electrical Engineering and Computer Science, University of Michigan, Ann Arbor, MI

NNIN REU Mentor(s): Brandon D. Lucas, Applied Physics, University of Michigan, Ann Arbor, MI

Contact: tesfaslassieim@appstate.edu, guo@eecs.umich.edu, bdlucas@umich.edu

Abstract:

This work focuses on the fabrication of Au nanoparticle arrays using nanoimprint lithography (NIL), and their application as biosensor transduction elements. Noble metal nanoparticles such as gold (Au) are unique in that upon illumination by light of certain frequency, collective oscillations of the free electrons can be produced. This characteristic response is known as the localized surface plasmon resonance (LSPR). Optical characterization of the nanoparticle arrays show that the LSPR is not only sensitive to nanoparticle shape and size but it is also sensitive to the surrounding dielectric medium. Therefore, a biomolecular binding event on the particle surface causes the LSPR spectral line to shift. Specifically in this project, the LSPR of Au nanoparticles is used to transduce the interaction between two non-structural proteins responsible for viral genome replication, NS3 and NS5. This goal was accomplished by implementing an immobilization strategy for purified His-tagged NS3 proteins to the nanoparticle surface using a nickel-nitrilotriacetic acid (Ni-NTA) surface chemistry.

Introduction:

Surface plasmons are collective electron-density oscillations generated on the surface of metallic films. As the resonant excitation of these plasmons is highly dependent on the dielectric function of the material on the metal surface, monitoring the resonance condition serves as a suitable method to transduce dielectric changes in the near-field of the metallic surface. Based on this principle, surface plasmon resonance (SPR) biosensors have been utilized extensively over the last decade to characterize various biomolecular systems. Most significant among the benefits of SPR is the ability to monitor biomolecular interactions in real-time without the need for various labels that can generate less robust signals and putative effects on the interaction of interest. An extension of this technique, known as localized surface plasmon resonance (LSPR), uses noble metal nanoparticles. LSPR is gaining interest in part due to the availability of more reliable fabrication methods, adaptability for use in commercially available spectroscopic systems and enhanced sensitivity. In this work, nanoimprint lithography (NIL) is utilized to produce plasmonic constructs that are optically characterized using microextinction spectroscopy. We subsequently utilize a surface-modified Au nanoparticle array to detect interactions between two non-structural proteins NS3 and NS5 which are found in a *Flavivirus replicase* complex.

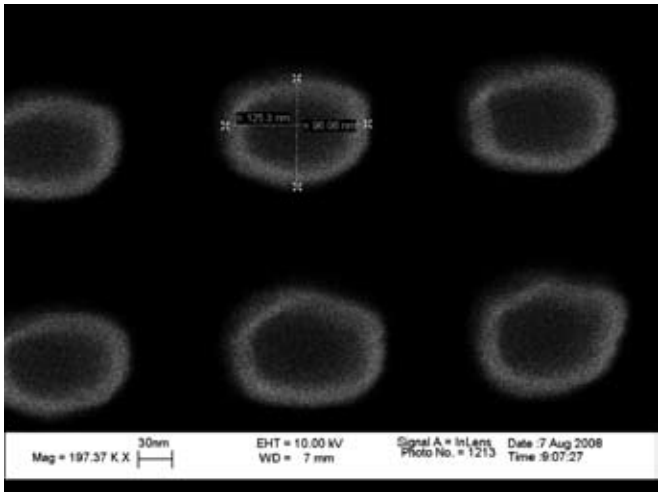

Figure 1: SEM of the nanoimprint mold.

Fabrication Process:

Nanoimprint lithography (NIL), a mold-based fabrication method, was used to fabricate nanoscale patterns on glass. Glass substrates were cleaned in a 1:1 piranha solution of H_2O_2:H_2SO_4 for 20 minutes followed by a rinse in deionized water solution and dried using N_2. Nanoimprint resist (MRi-8030) was spin-coated on the glass substrates to the appropriate thickness and then baked on a hot plate at 140°C for 5 minutes to remove residual solvent. A nanoimprinter (Nanonex, NJ) was used to imprint with a mold possessing an array of pillars with oval cross-sections (~ 130 nm by 100 nm) and gaps of ~ 90 nm (Figure 1) directly onto the prepared glass substrates.

The glass substrates were heated above the glass transition temperature of the nanoimprint resist (180°C) and pressure (670 psi) is used to create a conformal contact with the mold. After imprinting, a thin layer (~ 5 nm) of Ni was deposited using a shadow evaporation technique to promote undercutting and enhance the subsequent lift-off process. Residual layer removal was accomplished using a suitable O_2 plasma dry etching process (20 sccm; 50W; 20 mTorr). Following the etching, Au was deposited to the desired thickness on the glass substrates using an electron beam evaporator. Lift-off was performed by immersing the glass substrates in a beaker of acetone, and sonication when necessary. The finished samples were rinsed with methanol and IPA and dried with N_2. The resulting Au NP arrays were surface-modified with a Ni-nitrilotriacetic acid (Ni-NTA) surface chemistry in order to immobilize the purified His-tagged NS3 proteins onto the Au NPs. The surface modification technique was accomplished by the incubation of the Au NP substrates in solutions of cystamine, glutardialdehyde, Nα,Nα-bis(carboxymethyl)-L-lysine hydrate (NTA), and nickel sulfate respectively.

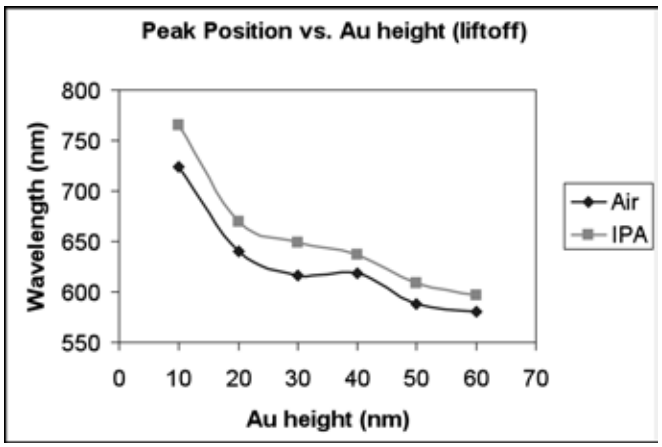

Figure 2: LSPR response of fabricated particle array (in air & IPA).

Experimental / Results:

The optical properties of the nanoparticles arrays were determined by an optical extinction measurement. These measurements were conducted using a Nikon TE300 Eclipse inverted microscope (40x objective) with transmitted broadband light focused into an optical fiber which was coupled to spectrometer (Ocean Optics HR4000). The SpectraSuite software package was used for all data acquisition and analysis. The first test was conducted on a variety of samples that were differentiated only by the height (10-60 nm) of the Au NPs. As shown in Figure 2, with increasing nanoparticle height there is a consistent resonance peak shift in the LSPR to shorter wavelengths (blue-shift). In addition, dielectric sensitivity was measured on the different heights by monitoring the LSPR response of the nanoparticles as

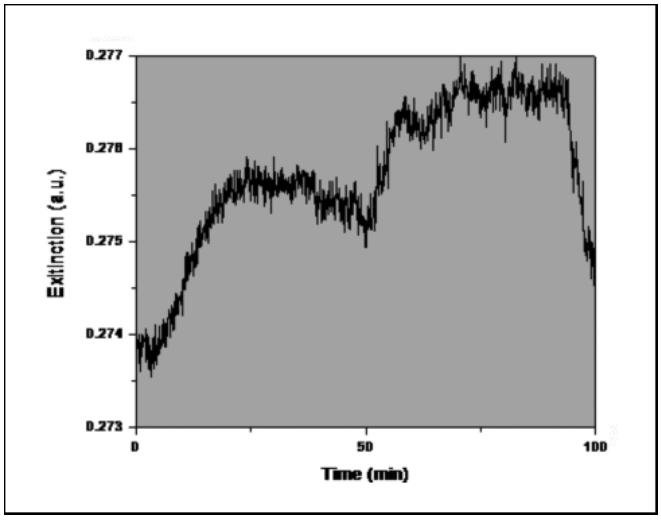

Figure 3: LSPR measurement of NS3 and NS5 interaction.

they interact with ambient air and isopropanol (IPA). Overall behavior shows an increase in wavelength (red-shift) with increasing refractive index. We observed that there is an optimal particle thickness (30 nm) that produces the highest environmental sensitivity.

Lastly, we tested the interaction of NS3 and NS5. A flow cell setup was used to flow NS3, NS3 buffer, NS5, and NS5 buffer respectively. As seen in Figure 3, the interactions of NS3 with the nanoparticle surface and with NS5 are clearly distinguishable based on the extinction vs. time graph (NS3 at ~ 0.0 min, NS3 buffer at ~ 25 min, NS5 at ~ 50 min, and NS5 buffer at ~ 75 min).

Conclusions / Future Work:

We successfully fabricated Au nanoparticles using NIL and have characterized their plasmonic properties. We applied our nanoparticles to detect interactions between NS3 and NS5. Optimization of the surface chemistry used to bind His-tagged proteins is being addressed and should lead to improved biosensor performance.

Acknowledgements:

I would like to thank Professor L. Jay Guo, Brandon Lucas, Dr. Sandrine Martin, Guo Nanogroup, Lurie Nanofabrication Facility, the National Science Foundation, Intel Foundation for funding, and the National Nanotechnology Infrastructure Network Research Experience for Undergraduates (NNIN REU) Program for all their help and support.

Integration of Biological Observations and Theory into Computer Simulations of Bacterial Binding

Suron Woods

Bioengineering, Oregon State University

NNIN REU Site: Center for Nanotechnology, University of Washington, Seattle, WA

NNIN REU Principal Investigator: Wendy Thomas, Bioengineering, University of Washington

NNIN REU Mentor: Matt Whitfield, Bioengineering, University of Washington

Contact: suronwoods@gmail.com, wendyt@u.washington.edu, mjwhit16@u.washington.edu

Abstract:

Some biological adhesive bonds, called catch bonds, are enhanced by tensile force which enables complex behaviors at the cellular level. For example, *Escherichia coli* bacteria, binding to mannosylated surfaces via a catch-bond forming protein called FimH, switch from transient to rolling to stationary adhesion as hydrodynamic shear stress is increased, and detach again if the flow is turned off. The behavior of the catch bond is also influenced by the mechanical structure of the bacteria.

Our lab currently uses adhesive dynamic simulations and computational analysis to examine the relationship between catch bonds under shear stress, the mechanical structure of the fimbriae, and the behavior of the bacteria in fluid flow. The goal of this project is to design and implement into the simulation the additional functionality of fimbrial uncoiling so that the affect of this behavior on the catch bonds as well as the behavior of the bacteria can be determined via computational analysis. We created a two-state Monte Carlo algorithm using the polymer Worm-Like-Chain equation to model the behavior of the fimbriae under shear force.

Introduction:

The first step in successful colonization and infection of many bacteria is adhesion to host tissues. *Escherichia coli* adheres to mannosylated surfaces via a catch-bond forming protein called FimH, which is located at the tip of its fimbriae, which are long rods composed of more than 1000 coiled FimA protein subunits forming a helical structure anchored to the outer bacterial membrane. These fimbriae exhibit spring-like uncoiling behavior under shear force which mediate the forces at the FimH tip and enhances bacterial adhesion.

Mechanical measurements done on fimbriae using atomic force microscopes show that fimbriae readily extend under applied force, caused by the uncoiling of the FimA protein subunits [1]. This uncoiling produces a force plateau region in the force extension curve which is optimized to mediate the shear forces at the FimH tip and enhances the catch-bond lifetimes, which in turn enhances bacterial adhesion [2].

In order for our adhesive dynamic simulations to accurately model the behavior of bacterial in fluid flow, the uncoiling behavior of the fimbriae must be accurately modeled in our simulation. Once the modeling of fimbrial behavior is incorporated into the simulation, we can use the simulations to explore the dynamics of the FimH catch bonds and their role in the adhesion of bacteria.

Procedure:

The behavior of fimbriae under shear force has previously been probed in atomic force microscope (AFM) experiments. The data from these experiments has been used to determine the structure and behavior of fimbriae under force, which can be modeled using the polymer Worm-Like-Chain equation. These experiments also produced force extension curve data that we can use to compare with our simulation data to determine the accuracy of our simulation model, as seen in Figure 1.

We created a two-state Monte Carlo algorithm to model the uncoiling behavior of fimbriae, and incorporated this into our simulation of bacterial behavior in fluid flow. Previous experiments have shown this type of algorithm best models the uncoiling behavior of fimbriae [3].

Our simulation models the fimbriae much like a two spring force scenario. Using the overall fimbrial extension and the number of subunits in each state (coiled and uncoiled), we set the two force equations equal to each other and solved for the total tensile force from the fimbriae using an iterative method. The algorithm then used that force to calculate the uncoiling of the FimA subunits based on the probability of uncoiling adjacent subunits. These fimbrial forces were then used to determine the behavior of the FimH catch bonds, and summed to determine the overall behavior of the bacteria in fluid flow.

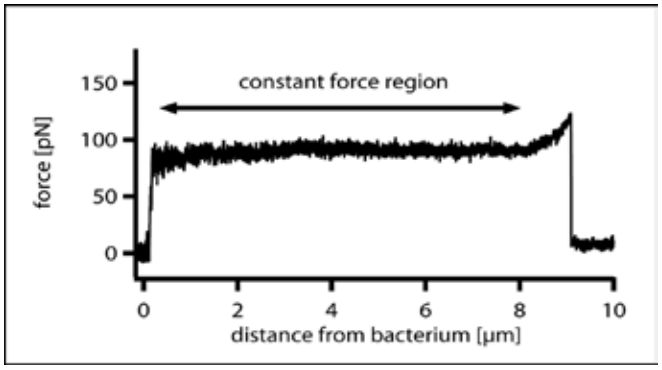

Figure 1: Force extension curve of uncoiling fimbriae from atomic force microscope experiments.

To determine the accuracy of our simulation, we ran the simulation using parameters to model a single fimbriae, and used the outputted simulation data to produce a force extension curve which we could compare to the data obtained from the AFM experiments.

Results and Conclusion:

Our simulation, resulting from modeling a single fimbriae, produced a force extension curve that matched the data obtained from AFM experiments. This was evidence that our simulation correctly modeled the behavior of single fimbriae under shear force. Thus, the simulation can be used to accurately describe and predict the behavior of bacteria in fluid flow, based on multiple fimbrial-surface interactions.

Future Work:

Our simulation can be used to run computational experiments to model the behavior of bacteria in fluid flow. Because these experiments are computational, we can alter parameters to explore the dynamics of fimbrial behavior, catch-bond interactions, and bacterial adhesion and behavior in fluid flow. In the future, this data may be used to fight bacterial disease or engineer adhesives that exhibit similar force dependant properties and behavior.

Acknowledgements:

I would like to thank the following for their assistance and support with this project: Wendy Thomas, Matt Whitfield, University of Washington Bioengineering Department, The National Nanotechnology Infrastructure Network Research Experience for Undergraduates Program, and The National Science Foundation.

References:

[1] Miller, Garcia, Hultgren, and Oberhauser. "The Mechanical Properties of E. coli Type 1 Pili Measured by Atomic Force Microscopy Techniques." Biophysical Journal 91 (2006): 3848-3856.

[2] Forero, Yakovenko, Sokurenko, Thomas, Vogel. "Uncoiling Mechanics of Escherichia coli Type I Fimbriae Are Optimized for Catch Bonds." PLOS Biology vol. 4 issue 9 e298 (2006): 1509-1516.

[3] Bjornham, Andersson. "Modeling of the elongation and retraction of Escherichia coli P pili under strain by Monte Carlo simulations." Eur. Biophysical Journal 37 (2008): 381-391.

Molecular Immobilization on a Gold Surface Using a Microfluidic Device

Justine Soo Yun Yoon

Biomedical Engineering, Rensselaer Polytechnic Institute

NNIN REU Site: Minnesota Nanotechnology Cluster, University of Minnesota-Twin Cities, Minneapolis, MN

NNIN REU Principal Investigator(s): Professor Sang-Hyun Oh, Electrical and Computer Engr, University of Minnesota

NNIN REU Mentor(s): Hyungsoon Im, Electrical and Computer Engineering, University of Minnesota

Contact: yoonj4@rpi.edu, sang@umn.edu, imxxx019@umn.edu

Abstract/Introduction:

In this study, surface plasmon resonance (SPR) imaging and microfluidics were combined to immobilize single stranded deoxyribonucleic acid (DNA) on a patterned gold surface, detect DNA hybridization, and measure molecular binding kinetics in a real-time, label-free manner. Single-stranded thiolated DNA (T-DNA) was first immobilized on a gold surface; thereafter, the complementary DNA (cDNA) strand and the non-complementary DNA (ncDNA) strand were injected through a polydimethylsiloxane (PDMS) flow cell [1]. Because there are multiple channels in the PDMS flow cell, different solutions were injected through each channel, rendering a multi-array sensor—the PDMS flow cell reduced the volume of the sample solution needed (which increases the diffusion rate) and decreased the overall size of the biosensor. The hybridization was detected through an SPR imaging technique, comprised of a collinear system in which an incident light is shone underneath the sensor [2]. The sub-wavelength nanoholes can efficiently convert incident photons into collective oscillations of conduction electrons, known as surface plasmon (SP) waves at the gold surface. These surface plasmon waves propagate throughout the surface, and re-radiate as a sharp transmission of light at the other surface end. This transmission was detected by a couple charge device (CCD) camera and was shown as an intense transmission peak (peak position depends on the periodicity of the array and the refractive index surrounding the gold surface). If there were molecules present on the surface of the array, there would be a decrease in transmission intensity, resulting in a shift of the peak. Fluorescently tagged cDNA was used to verify the hybridization of DNA using a fluorescence array scanner. This technique can be used, in part, for gene mutation screenings as well as molecular interaction studies. The results showed that hybridization was possible through a microfluidic device and that a transmission peak could be detected through the biosensor.

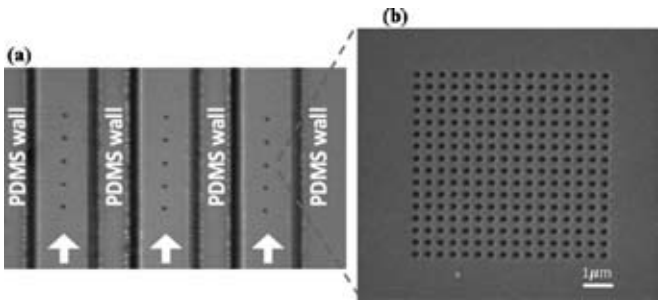

Figure 1: (a) Bright field image of a PDMS channel. (b) SEM image of nanohole array milled by a focus ion beam (200 nm diameter and 400 nm period).

Experimental Procedure:

Using an electron beam evaporator, 5 nm of chromium, followed by 100 nm of gold, were deposited onto a clean glass slide, and placed in an ozone oven for ten minutes. Next, a 3×5 array of 16×16 nanoholes, (200 nm diameter and 400 nm periodicity), was milled onto the surface of the slide using a focused ion beam (Figure 1).

The fabricated microfluidic device used photolithography to construct three channels (each channel 100 μm wide and 50 μm deep) (Figure 2a) by spinning SU-8 photoresist onto a blank four inch silicon wafer at 2000 rpm for 30 seconds. The wafer was then prebaked, soft-baked, exposed to ultraviolet light under a patterned chrome mask, baked again, and developed [1]. Next, it was coated with a self-assembled monolayer of alkanethiols using a vacuum chamber. A 10:1 mixture of PDMS and curing agent was poured onto the wafer, and cured. Finally, six holes (1 mm diameter), were punctured into the inlets and outlets.

After preparing the reagents in Table 1, 30 μl of T-DNA were pipetted onto the surface of the slide over the nanoholes, incubated in a 37°C humid chamber, and rinsed. The T-DNA area was then treated with 90 μL of mercaptohexanol, incubated, and washed. The PDMS flow cell was coated with bovine serum albumin, incubated, and rinsed. A glass cover slide was placed over the PDMS and gold slide and secured by mechanical bonding, where tubes (0.05 inches in diameter and 3 inches long) were inserted into the inlets and outlets (Figure 2a and b). Finally, fluorescent/complementary-DNA (F/cDNA) was injected into the right channel, fluorescent/non-complementary-DNA (F/ncDNA) into the left channel, and the center channel was left empty. After a 24 hour incubation period in the humid chamber, the fluorescent labels were detected using a fluorescent microarray scanner.

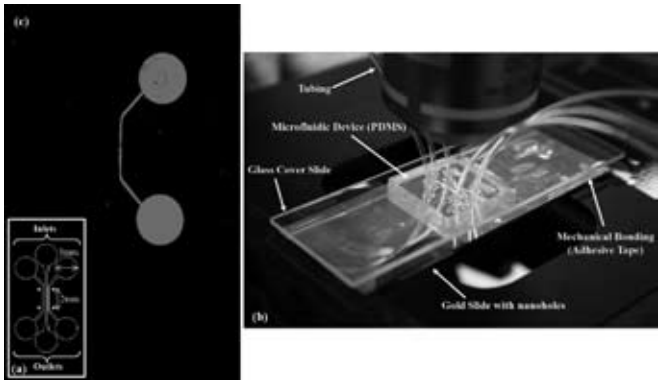

Figure 2: (a) Schematic of PDMS flow cell. (b) Complete SPR sensor. (c) Result from fluorescence array scanner. Right channel (F/cDNA), Left channel (F/ncDNA), Center channel (empty).

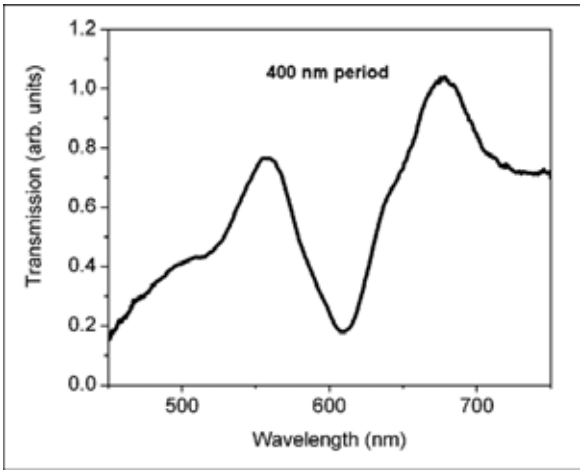

Figure 3: Transmission spectrum. The sharp peak shifts when DNA binds to the surface.

Results and Conclusions:

After several trials, DNA hybridization in a PDMS flow cell was successful. Figure 2c shows the fluorescence of the positive control channel. The main problem encountered for the first several trials revolved around the F/cDNA leaking out of its channels and into other channels; this error could be attributed to air bubbles or impurities between the PDMS flow cell and gold slide, or the flow rate of F/cDNA. Since DNA is hydrophilic, it is more prone to spread on the surface rather than stay within the channel walls. This leakage problem was corrected using a contact aligner to apply the flow cell to the gold surface—a uniform pressure over a wide area was applied onto the PDMS and the gold slide ensuring a tight seal. Figure 3 shows a transmission spectrum of the nanohole arrays without any molecules on the surface. The two peaks are due to the different periodicities between the adjacent hole, and the diagonal hole.

Future work would include the injection of DNA and complementary DNA through the flow cell while simultaneously measuring the transmission to see if the imaging system could detect the hybridization.

Acknowledgments:

The author would like to acknowledge Professor Sang-Hyun Oh, Hyungsoon Im, Nathan Lindquist, Antione Lesuffleur, Kwan Seop Lim and Si-Hoon Lee for the opportunity to work alongside them in their lab and for all their guidance. She would also like to thank the National Nanotechnology Infrastructure Network Research Experience for Undergraduates (NNIN REU) Program and NSF for funding this experiment.

References:

[1] Sia, S.K., Whitesides, G.M.; "Microfluidic devices fabricated in Poly(dimethylsiloxane) for biological studies"; Electrophoresis, 24, 3563 – 3576 (2003).

[2] Lesuffleur, A., Im, H., Lindquist, N. C., Lim, K. S., and Oh, S.; "Laser-illuminated nanohole arrays for multiplex plasmonic microarray sensing"; Opt. Express. 16, 219-224 (2008).

Stock solution	T-DNA	F/C-DNA	F/N-CDNA	DNA
100 mM Tris-HCl	12.5 mM	10 mM	10 mM	10 mM
10 mM EDTA	1.25 mM	1 mM	1 mM	1 mM
5 M NaCl	0	1M	1M	1M
10 mM TCEP	1.25 mM	0	0	0
20 µM T-DNA	1.25 mM	0	0	0
20 µM F/C-DNA	0	1 µM	0	0
20 µM F/NC-DNA	0	0	1 µM	0
20 µM DNA	0	0	0	1 µM
DI-UV Water	*	*	*	*

*Table 1: Reagents used * Volume varies depending on total solution volume.*